DIELECTROPHORETIC FORCE STIMULATION FOR BONE FRACTURE HEALING

by

Erman Kibritoğlu

BSc, Electrical and Electronics Engineering, Yeditepe University , 2010

Submitted to the Institute of Biomedical Engineering
in partial fulfillment of the requirements
for the degree of
Master of Science
in
Biomedical Engineering

Boğaziçi University
2013

DIELECTROPHORETIC FORCE STIMULATION FOR BONE FRACTURE HEALING

APPROVED BY:

Prof. Dr. H. Özcan Gülçür ..... (Thesis Advisor)

Prof. Dr. Nurettin Heybeli .....

Assoc. Prof. Dr. Albert Güveniş .....

DATE OF APPROVAL: 19 June 2013

Acknowledgements

I dedicate my thesis to my grandfather Dr. Mehmet Sarıkaya who always supported and encouraged me during my education life.

Abstract

DIELECTROPHORETIC FORCE STIMULATION FOR BONE FRACTURE HEALING

On the average, a person has two bone fractures during a lifetime. The healing time depends on the age, the health of the patient, the type and the severity of the fracture and can be quite long, especially if there is an infection. This is very frustrating for patients during this time, since they require help and are unable to work. Although a number of invasive and non-invasive techniques have been studied for shortening fracture healing times, including the application of direct current, electromagnetic fields, pulsed electromagnetic fields, ultrasound and low-intensity x-ray. However none of these techniques are entirely satisfactory. In the present thesis we propose a novel technique based on the use of dielectrophoretic forces (DEPFs).

By applying a non-uniform electromagnetic field around a fracture site, red blood cells within the blood will be polarized, creating electrical dipoles. Due to the interaction of these dipoles and the electromagnetic field, the red blood cells will be subjected to dielectrophoretic forces that will accelerate them and thus the blood flow will be increased. This will, in turn, increase vascularization, transmembrane signalling, the supply of nutrients, necessary hormones and growth factors at the fracture site and thus help bone healing.

For the generation of non-uniform fields we considered three different coil designs (linear, parabolic and square root). Using Mathcad we numerically studied extensively, the dielectrophoretic forces for a long bone fracture where the main arteries are vertically-oriented and the blood flow is downward. The gravitational force and the drag force on the red blood cells determine the steady state blood flow. The dielectrophoretic force added to the force balance is functional in increasing the blood flow.

The ratio of the velocity in the presence of dielectrophoresis to the velocity without dielectrophoresis (called here as the Dielectrophoretic Force Factor, κ_{DEPF}) is a good measure of the performance of the dielectrophoresis, since it indicates the increase in blood flow. It was found that the dielectorophoretic force reaches the peak levels at a frequency range between 5-15 Hz. At 5 Hz, the average value of κ_{DEPF} is 1.90, 2.51 and 1.61 for the linear, parabolic and the square root coils, respectively. Thus, the parabolic coil seems to be the best choice for bone healing.

Keywords: Bone fracture healing, dielectrophoretic force, red blood cell.

Özet

KEMİK KIRIĞI İYİLEŞMESİ İÇİN DİELEKTROFORETİK KUVVET UYARIMI

Ortalama olarak, bir insanın hayatı boyunca iki kez kemik kırığına rastlanmaktadır. İyileşme süresi hastanın yaşına, sağlığına, kırığın tipine, şiddetine ve özellikle bölgedeki enfeksiyona göre çok uzun olabilmektedir. Hasta çalışamaz durumda ve yardıma ihtiyacı olduğu için bu durum hasta için yıpratıcı olmaktadır. Kırık iyileşme süresini azaltmak için invaziv ve noninvaziv yöntemler üzerinde çalışılmasına rağmen, doğru akım, elektromanyetik alan, darbeli elektromanyetik alan, ultrason ve düşük yoğunluklu x-ışını gibi, bu yöntemlerin hiçbiri tatmin edici olmamıştır. Bu tezde, yeni bir yöntem olan dielektroforetik kuvveti anlatmaktayız.

Kırık bölgesine sabit olmayan elektromanyetik alan uygulanarak, kırmızı kan hücreleri kutuplaştırılabilir ve elektrik dipolleri oluşturulabilir. Bu dipollerin birbiriyle etkileşimi ve elektrik alandan dolayı kırmızı kan hücreleri dielektroforetik kuvvete maruz bırakılacaktır ve hızlanacaklardır, böylece kan akışı hızlanacaktır. Ayrıca, bu hızlanma sayesinde kırık bölgesinde damarlanma artışı, transmembran sinyallenmesi, besin maddeleri ve büyüme faktörlerinin artışı olacak, böylece kırık iyileşmesine yardımcı olunacaktır. Kırmızı kan hücreleri üzerindeki yerçekimi ve sürtünme kuvveti kan akışının kararlı halde olmasını sağlamaktadır. Dielektroforetik kuvvet bu kuvvet dengesine eklenerek kan akışı hızlandırılabilir.

Sabit olmayan elektromanyetik alanın üretilmesi için üç farklı bobin modeli düşünülmüştür (doğrusal, parabolik ve karekök). Mathcad kullanılarak numerik olarak detaylı çalışılmıştır. Uzun kemik kırığı civarında ana arterler dikey odaklı ve dielektroforetik kuvvet kan akışı yönünde aşağıya doğrudur.

Kan akış hızının artışını göstermek için dielektroforesiz (Dielektroforetik Kuvvet, κ_{DEPF}) varlığında olan akış hızının dielektroforesiz olmadanki akış hızına oranı iyi bir ölçü olmaktadır. Dielektroforetik kuvvet 5-15 Hz aralığında doruk noktasına ulaşmaktadır. 5 Hz için ortalama κ_{DEPF} doğrusal, parabolik ve karekök bobinler için sırasıyla 1.90, 2.51 ve 1.61 dir. Böylece parabolik bobin kırık iyileşmesi için en iyi seçenektir.

Keywords: Kemik kırığı iyileşmesi, dielektroforetik kuvvet, kırmızı kan hücresi.

Table of Contents

List of Figures

List of Tables

List of Symbols

ϵ_m	Permittivity of surrounding medium
ϵ_0	Permittivity of particle
ϵ_m^*	Complex permittivity of surrounding medium
ϵ_0^*	Complex permittivity of particle
ϵ_0^*	Complex permittivity of particle
ϵ_0^*	Complex permittivity of particle
$\triangle\epsilon_n$	Relative dielectric permittivity
$\epsilon_r^{'}$	Complex magnitute of dielectric constant
$\epsilon_r^{''}$	Complex magnitute of dielectric constant
ω	Angular frequency
E	Electric field
$K(\omega)$	Clausius mossotti factor
$\bigtriangledown$	Gradient operator
$\bigtriangledown\times$	Curl operator
$\Re$	Real part
$\Im$	Imaginary part
σ_ℓ	Conductivity
λ	Relaxation time
j	Imaginary unit
$K(k)$	Elliptic integral of the first kind
$E(k)$	Elliptic integral of the second kind
$\vec{B}$	Magnetic field vector
$\vec{B_r}$	Magnetic field vector in the r direction
$\vec{B_z}$	Magnetic field vector in the z direction
$\vec{B_{phi}}$	Magnetic field vector in the phi direction
μ_0	Permeability constant
η	Viscosity
ρ_{rbc}	Density of red blood cell

ρ_{plasma}	Density of blood plasma
V	Velocity
g	Gravitational Constant
f	Frequency
I	Current
r	Radius of coil

List of Abbreviations

$DEPF$	Dielectrophoretic Force
MSCs	Mesenchymal stem cells
MFI	Magnetic field intensity
$TGF\beta$	Transforming growth factor beta
BMPs	Bone morphogenic proteins
IGFs	Insulin like growth factor
PDGFs	Platelet derived growth factor
FGFs	Fibroblast growth factor
DEP	Dielectrophoretic
n-DEP	Negative dielectrophoretic
p-DEP	Positive dielectrophoretic
AC	Alternative current
DNA	Deoxyribonucleic acid
RNA	Ribonucleic acid

1. INTRODUCTION

1.1 Motivation and Background

On the average, a person has two bone fractures during a lifetime [1]. They are caused by a fall, blow, or other traumatic events in which the physical force exerted on the bone is stronger than the bone itself.

The risk of fracture depends, in part, on age. Fractures are very common in childhood. However children's fractures are, in general, less complicated than fractures in adults. Elder people are more likely to suffer fractures from falls that would not occur when the bones were young, because with age bones become more brittle. Osteoporosis, a disorder in which the bones become thin and loose strength as they age, causes 1.5 million fractures each year in the U.S., especially in the hip, wrist, and the spine. Besides osteoporosis, there are many other diseases (such as cancer) that weakens the bones and cause pathologic fractures that can occur with little or no trauma [2].

The severity of a fracture depends upon its location and the damage done to the bone and the tissue near it. Serious fractures can have dangerous complications if not treated promptly. Possible complications include damage to the blood vessels or nerves and infection of the bone (osteomyelitis) or the surrounding tissue. Recuperation time varies depending on the age and health of the patient and the type of the fracture. A moderate fracture in a child may heal within a few weeks whereas a similar fracture in an older person may take months to heal. In some cases, to correct a limb deformity, congenital or acquired shortened stature (due to accident, polio, wrongly united fracture, crush injury, pus formation in bone or bone gap) the bone may be deliberately fractured. By using a cage like frame around the limb and wires or needles passing through the targeted bones, the bone may be elongated several centimeters. Known as the Ilizarov Technique, a bone growth of 0.1cm/day can be achieved. The patient has to be in the frame for months.

These long healing times are very frustrating for patients. They usualy require help and are unable to work. Scientists have therefore been studying techniques for shortening fracture healing times using a variety of means including electromagnetic fields.

Bone healing creates a demand for blood flow in tissues that are near the fracture site. Development of the vascular tissue and the initiation and propagation of the periosteal response are the prominent driving mechanism of bone regeneration. Vessel formation depends on sufficient blood flow. It has been well established that the increase of blood flow near the fracture site accelerates vessel formation and bone regeneration; a fracture may heal faster if there is an increase in the blood flow near the fracture site.

A variety of techniques, including electrical stimulation, have been tried to facilitate fracture healing. For example, it has been shown that stimulation by direct current or ac current have beneficial effects. The exact mechanism by which electrical stimulation improves bone repair is still not fully understood. It needs more investigation. However, to date, direct current has been documented to work by an electrochemical reaction at the cathode. Capacitive coupling and inductive coupling have shown to work by alteration of growth factors and transmembrane signalling. Further studies are needed to support and optimize electrical stimulation for bone healing [3].

Mankind's use of electromagnetic fields for therapy may date back to the times naturally magnetized pieces of the mineral magnetite (called lodestone) was first discovered. In Middle English lodestone means 'course stone' or 'leading stone', showing its importance to early navigation. In the 15th century, Swiss physician and alchemist Paracelsus used lodestones to treat epilepsy, diarrhea, and hemorrhage. In the late 18th century, the Austrian physician Franz Anton Mesmer, who originated the idea of "animal magnetism", described healing properties of passing magnets over the open veins of patients [4]. In the mid-19th century, magnetic ointments produced in New York were introduced as remedies for a whole spectrum of illnesses such as headaches, inflammation of the bowels, burns, fever sores, rheumatism, gout, and toothache. Al-

though electricity's potential to aid bone healing was reported as early as 1841, it was not until the mid-1950s that scientists seriously studied the subject.

In the past 25 years or so, many researchers have investigated techniques for promoting the healing of bone defects in both human beings and animals. For example, the application of direct current, in the order of 20 microamperes, at the site of a fracture is known to promote bone growth and thus healing. The cathode is usually applied at the site of the defect; the anode is placed somewhere in the adjacent tissue or on the skin of the patient. While such arrangements are totally or partially invasive, non-invasive techniques are also in use; an externally generated electromagnetic field is caused to pass through the fracture site, thus inducing a current which promotes healing. The first approach suffers from the disadvantage of being at least partially invasive, while the second suffers from the disadvantage of requiring precise alignment of coils relative to the area to be treated as well as constant attention of medical personnel. Furthermore, many months are usually required to achieve healing when using any of the prior methods.

Fukada's and Yasuda's discovery of the electric potential of bone provides evidence of electricity's effect in promoting osteogenesis (bone growth), particularly in long bone non-unions [5]. During the 1970s, Bassett and his team introduced a new approach for the treatment of delayed fractures, a technique that employed a very specific biphasic low frequency signal to be applied for non-union and delayed fractures [6]. The use of electrical stimulation in the lumbosacral region was first attempted by Alan Dwyer of Australia [7]. In 1974, he reported successful initiation of graft incorporation in 11 of 12 fusion patients. Electrical stimulation has been shown to significantly increase the probability of bony arthrodesis in spinal fusions [8]. In 1979 FDA approved non-invasive devices using pulsed electromagnetic fields designed to stimulate bone growth. In 2004, a pulsed electromagnetic field therapy (PEMFT) system was approved by FDA as an adjunct to cervical fusion surgery in patients at high risk for non-fusion [9]. The use of PEMFT has been found to be safe. It has also been proven safe and effective in treatment of delayed union in long bone fractures and patients at risk of non-union following spinal fusion surgeries [10].

Pulsed electromagnetic field therapy, also called pulsed magnetic therapy, pulse magnetotherapy, is a reparative technique most commonly used in the field of orthopedics. In the case of bone healing, PEMF uses electrical energy to direct a series of magnetic pulses through injured tissue whereby each magnetic pulse induces a tiny electrical signal that stimulates cellular repair. Many studies have also demonstrated the effectiveness of PEMF in healing soft-tissue wounds; suppressing inflammatory responses at the cell membrane level to alleviate pain, and increasing range of motion. The value of pulsed electromagnetic field therapy has been shown to cover a wide range of conditions, with well documented trials carried out by hospitals, rheumatologists, physiotherapists and neurologists. There are several electrical stimulation therapy devices, approved by the FDA, that are widely available to patients for use. These devices provide an additive solution that aid in bone growth repair and depression [11].

The techniques described above are not entirely satisfactory and there is a great need for the development of better techniques. In the present thesis we introduce a new technique based on the use of dielectrophoretic forces. This explained in the next sections.

1.2 Objectives

Adequate blood flow is vital for bone fracture healing, since blood carries necessary hormones and growth factors to the fracture site. Clearly, fracture healing can be accelarated by increasing the blood flow. In this thesis, we investigate how this can be achieved using dielectrophoretic forces.

If we can generate a non-uniform electric field around the fracture site, red blood cells within the blood can be polarized, creating electrical dipoles. Due to these dipoles the red blood cells will be subjected to (dielectrophoretic) forces that will accelerate them and thus increase blood flow. The objective of this thesis is to study how these non-uniform fields can be generated and how dielectrophoresis may help fracture healing. For the creation of the required non-uniform fields, we considered

three different coil models, namely, the linear, the parabolic and the square root coils. Using Mathcad we studied the dielectrophoretic forces extensively. An outline of this work is given in the following section.

1.3 Outline of The Thesis

The remaining chapters are organized as follows. Chapter 2 introduces briefly, the physiology of bone fracture healing. Types of fractures and bone formation mechanisms are discussed here. Dielectrophoresis is discussed in Chapter 3. Chapter 4 covers numerical analysis of dielectrophoresis for linear, parabolic and square root coil models. Chapter 4 ends with a discussion. Appendix A explains the derivation of dielectrophoretic force. Appendix B gives numerical calculations of dielectrophoretic forces.

2. BONE FRACTURE HEALING

2.1 Introduction

Bone is a stiff composite material and consists of fibrous protein collagen. It is absorbed with rich calcium phosphate. Also, the bone is covered by living cells and blood vessels within it. Inside the bone, there are hematopoietic cells known as bone marrow [12].

Bones consist of two structures as cortical bone and cancellous bone. The Cortical bone is the outer layer of the bone. It resists bending. Haversian system (osteon) is the fundamental functional unit of compact bone. In the middle of the osteon there is a Haversian canal that has blood vessels, loose connective tissue and nerves. Also, each osteon is connected with each other by Volkmann's canals. In addition, in the osteon there are osteocytes which are present in the lacunae and interconnected by canaliculi. Haversian canals are the nutrient supplier of the bones and through the Volkmann's canals, the system is connected through all around the bone.

Cancellous bone consists of trabeculae and collagen fibers which are present in trabeculae. The collagen fibers are located as parallel lamellae. The outer layer of trabeculae consists of flattened cells and inside trabeculae there are osteoblasts [13].

Periosteum is the outer layer of the bone and it consists of collagen fibers, fibroblasts and osteoprogenitor cells that can make mitotic divisions to differentiate into osteoblasts. They are necessary for the healing and the growth of the bone. They are known as bone forming cells. Because of this osteoblasts synthesize organic components of the bone matrix. When it is active it shows alkaline phosphate activity [13].

2.2 Bone Formation Mechanism

There are five stages of bone remodeling:

- Quiescence
- Activation
- Resorption
- Reversal
- Formation

The resting state of a bone surface is known as the quiescence stage. In this stage, all of the bone surface is in the resting state. Later, activation stage starts in which, osteoclasts are recruited to the surface of the bone. The osteoclasts regulate coupling to osteoblasts by reducing the bone formation activity during the bone remodeling. The third stage of the bone formation is resorption; it is the removal of the bone by the osteoclasts. After this stage, the osteoclasts stop removing the bone and the osteoblasts fill the defect. Finally, in the formation phase the bone is layed down by the osteoblasts [14].

Figure 2.1 shows the bone lining cells and the endosteal membrane (quiescent phase), retraction of the cells and the membrane resorption (activation phase), activity of the osteoclasts (resorption phase), matrix of the osteoblasts and osteoid (formation phase), mineralization of the bone tissue and finally the bone structure unit (quiescent phase).

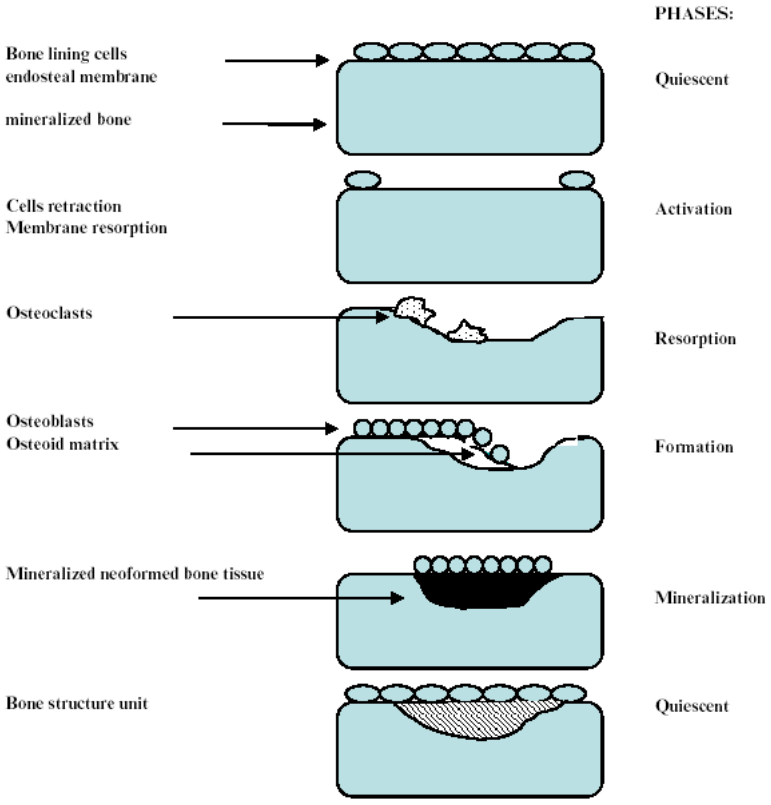

Figure 2.1 Bone formation mechanism [15].

2.2.1 Periosteal Bone Formation

In the periosteal bone formation, tissue vascularizition is increased, mesenchymal stem cells are proliferated to differentiate into osteoblasts, osteoblasts start to lie down into the osteoid which is the organic part of the bone. In the osteoids, osteoblasts turn into osteocytes. The osteoids are calcified to form the cancellous bone. The periosteum and the compact bone are formed [16]. Figure 2.2 shows the outer and inner structure of a bone.

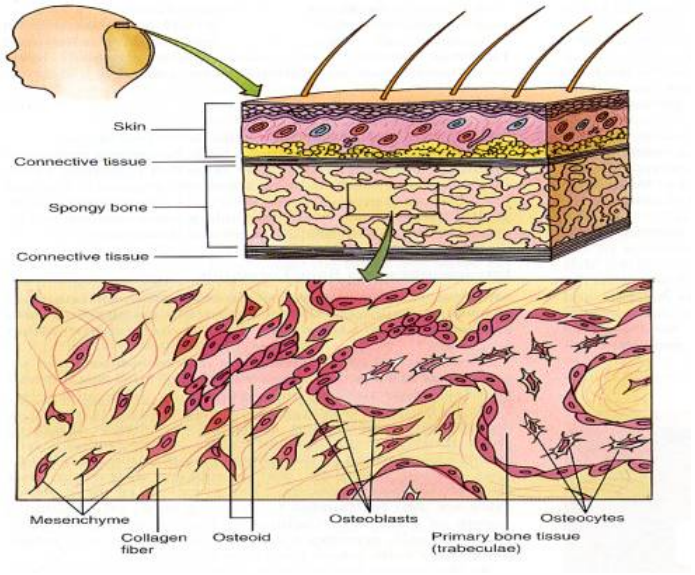

Figure 2.2 Periosteal bone formation [17].

2.2.2 Endochondral Bone Formation

Endochondral bone formation is an essential process during the healing of the bone fractures. There are two stages of process in endochondral bone formation. In the primary center of ossification, perichondrium becomes periosteum which contains osteopregenitor cells that later become osteoblasts. Then, the osteoblasts secrete osteoid against the shaft of the cartilage model which serves as support for the new bone. Also, chondrocytes begin to grow in this stage that is known as hypertrophy. They stop secreting collagen and other proteoglycans and begin secreting alkaline phosphatase that is needed for mineral deposition. Besides, calcification of the matrix occurs and apoptosis of the hypertrophic chondrocytes takes place. This creates cavities in the bone. The hypertrophic chondrocytes secrete vascular endothelial cell growth factor that induces growth of the new blood vessels from the perichondrium. The blood vessels from the periosteal bud invade the cavity left by chondrocytes and branch in the opposite directions along the length of the shaft. The blood vessels carry hemopoietic cells, osteoprogenitor cells and the other cells inside the cavity. Hemopoietic cells will later form the bone marrow. Then, osteoblasts that are differentiated from the osteoprogenitor cells enter the cavity by means of the periosteal bud. Besides, it secretes osteoid which then creates trabecula of the bone. In addition, osteoclasts break down the

cancellous bone to form the bone marrow cavity [18]. In the secondary center of ossification, the cartilage between the primary and secondary ossification centers is called the epiphyseal plate and it continues to form the new cartilage which is replaced by the bone. It results in an increase in the length of the bone [19].

2.3 Blood Supply of Long Bone

Long bones have three blood supplies. These blood vessels carry the necessary nutrients to the bone. The nutrient artery is the main blood supply of the bone. It enters the long bone to form the medullary arteries up and down. The periosteal arteries arise to from the capillary rich periosteum. In case of injury, it is capable of supplying a much greater proportion of the cortex to the medullary blood supply. Lastly, the metaphyseal arteries arise from the periarticular vessels. It penetrates the thin cortex in the metaphyseal region and anastomose with the medullary blood supply [13].

Bone healing creates a demand for blood flow in tissues that are near the fracture site. Therefore, the bone regeneration occurs. Development of the vascular tissue and the initiation and propagation of the periosteal response are the prominent driving mechanism of the bone regeneration. The effect of the vessel formation depends on the sufficient blood flow. In fracture healing, it has been well established. So, increase in blood flow near fracture site accelerates the vessel formation and the bone regeneration. Growth factors play an important role in the bone formation. The member of the transforming growth factor beta (TGFβ), bone morphogenic proteins (BMPs), insulin like growth factors (IGFs), platelet derived growth factors (PDGFs) and fibroblast growth factors (FGFs) make an osteoinductive effect. After haematoma is formed, resulting from injury to the periosteum, platelets aggregate on the fracture site and start stimulating the release of growth factors. In the bloodstream there are growth factors and hormones like parathyroid hormone, calcitonin, insulin, growth hormone, glucocoticoids, sex steroids and thyroid hormone. These hormones are significant in the bone formation [16]. Figure 2.3 shows the healing process of a bone fracture.

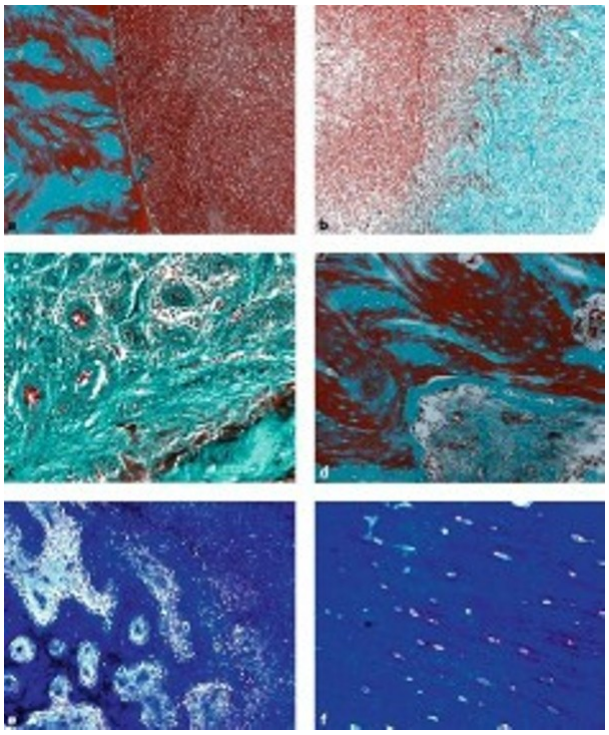

Figure 2.3 a Blood clot formation b Substitution of blood cells by a matrix rich repair tissue c Invasion of blood vessels d Organization of predetermined osseous tissue e Trabaculae formed by osteoblasts f Final repair tissue [16].

2.4 Mesenchymal Stem Cell in Bone Development and Repair

Mesenchymal stem cells form the stroma component of bone marrow. It supports hematopoiesis and bone formation [20]. As hematopoetic cells, mesenchymal stem cells (MSCs) are multipotent and they are derived from the bone marrow. They have the capability to develop into many cells such as bone, cartilage, tendon, muscle, marrow, fat and dermis. During embriyogenesis MSCs condensate and differentiate to form cartilaginous that is the anatomical model of the future bones. There are several phases for MSCs to develop into other kinds of cells. MSCs are the continious supply of the osteogenic cells that are required for the fracture healing [21]. Systemic hormones and growth factors regulate the bone physiology and their effect is transduced by cellular transcription machinery to regulate the differentiation process [22, 23]. Figure 2.4 shows the pluripotent behaviour of MSCs.

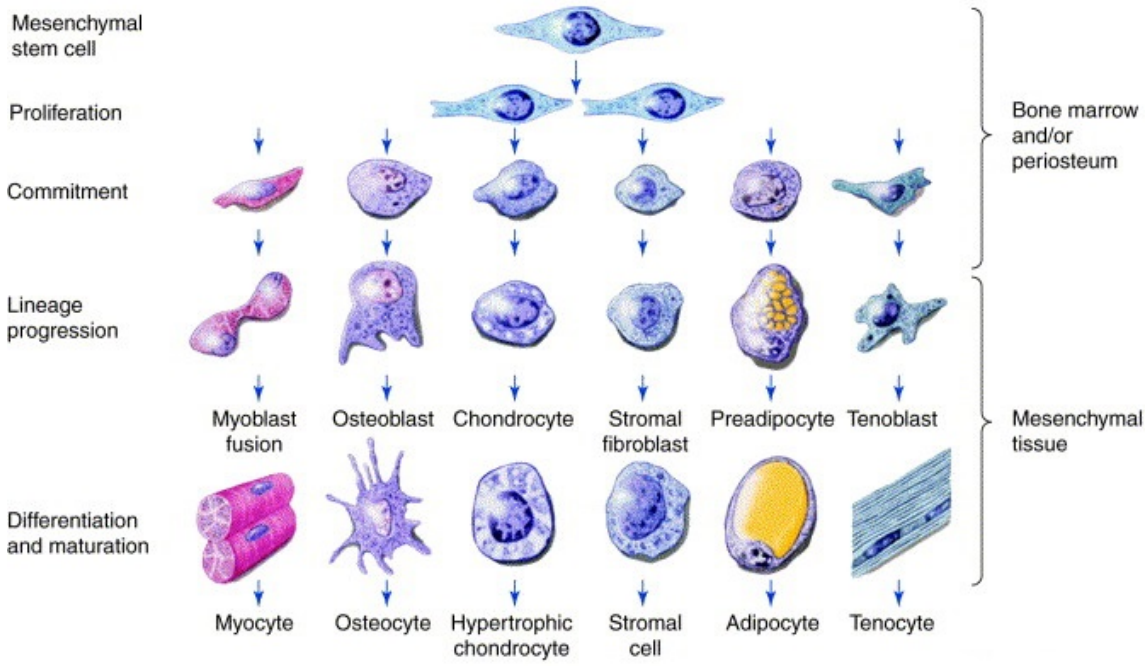

Figure 2.4 Mesengenic process [24].

2.5 Function of The Sex Hormone Binding Globulin

It was proven that the stromal cells isolated from bone marrow can be stimulated by glucocorticoids to differentiate into the mature preosteoblastic cells [25]. Differentiation of mesenchymal stem cells to osteoblasts appears in the following order: accumulation of the collagenous matrix, expression of the alkaline phosphatase, secretion of the osteocalcin and finally mineralization of the bone [26]. It has been suggested that the steroids such as estrogen may play a key role in the differentiation mechanism of mesenchymal stem cells [27]. Many studies suggest that estrogen hormone can directly improve the osteoblastic activity and the bone formation [28, 29, 30]. The effect of estrogen on proliferation and differentiation of osteoblastic cells in the bone marrow cultures has been investigated. During the first six days of the culture the effect of estrogen has been under survey. The number of cells grown in the presence of estrogen was significantly higher on day six when compared with control cultures that are grown during the absence of estrogen hormone [31].

In the blood circulation, the steroids bound to the plasma proteins, yet only the unbound steroids are able to enter the cell. Target cells respond specifically to

physiological levels of the steroid. They differ from the non-target cells that are able to synthesize a receptor proteins that are responsible for the uptake of the steroid. Besides, the steroid protein complex is then transferred into the nucleus, then the process causes some alterations in the complex. Inside the nucleus, the complex is bound to a specific part of the nucleus chromatin at the acceptor sites. RNA polymerase takes action to start transcription of the specific part of DNA, thus protein synthesis in the ribosomes occurs [32].

3. METHODS

3.1 Dielectrophoretic Force for Spherical Particles

Dielectrophoresis describes forces exerted on a particle when it is placed in a non-uniform electric field and the particle and the surrounding medium have different polarizabilities such as different dielectric permittivity, conductivity, relaxation time, etc. A charged particle placed in a uniform electric field will be subjected to a force. A neutral particle in the same uniform field will not be effected because each half of the induced dipole in this particle will be subjected to opposite and equal forces which cancel each other out. However, in a non-uniform electric field a neutral particle polarizes and the two halves of the induced dipole are subjected to different force magnitudes which altogether is known as the *dielectrophoretic force* (DEPF). It is important to emphasize that the electrophoretic force can be applied to charged particles, yet the DEPF does not require charged particles in order to manipulate it. The particle has to only differ electrically from the medium. In addition, AC excitation reduces membrane polarizability [33]. Spherical like structure of hemoglobin allows to use the DEPF [34].

Dielectrophoretic force equation for spherical particles is:

$$F = 2\pi r_p^3 \epsilon_0 \epsilon_m \Re\left[K\left(\omega\right)\right] \nabla\left(E^2\right) \tag{3.1}$$

where ϵ_m *and* ϵ_0 are the permittivity of the surrounding medium and air respectively, r_p is the radius of the particle that is aimed to manipulate, ω is the radian frequency of the field, E is the electric field and $K\left(\omega\right)$ is the clausius-mossotti factor [35].

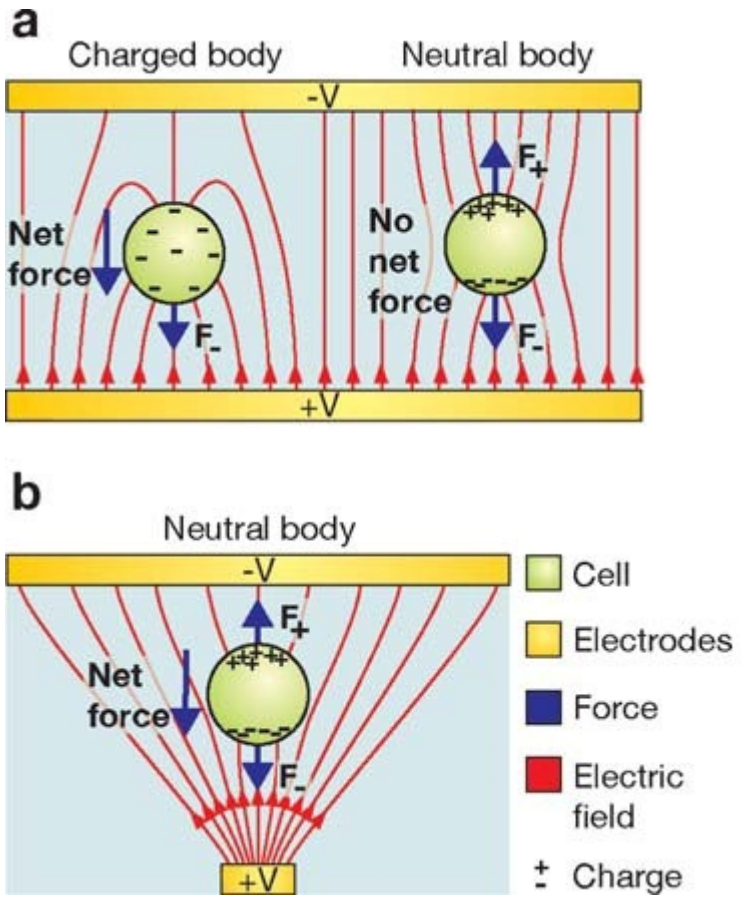

Figure 3.1 a Uniform electric field for charged and neutral body b Non-uniform electric field for neutral body [35].

In Part a of Figure 3.1, a uniform electric field is applied to the charged and neutral bodies. Charged body moves in the opposite direction of the electric field, yet the neutral body does not move because opposite forces cancel each other.

In Part b, a non-uniform electric field is applied to the neutral body and a net force is created. The particle moves in the direction of the dielectrophoretic force.

3.1.1 The Clausius-Mossotti Factor

The Clausius-Mossotti factor gives the frequency dependence of the DEPF. The negative Clausius-Mossotti factor means the negative dielectrophoretic force (n-DEPF) and a positive Clausius-Mossotti factor refers to the positive dielectrophoretic force (p-DEPF) [35].

The Clausius Mossotti factor is:

$$K(\omega) = \frac{\epsilon_p^* - \epsilon_m^*}{\epsilon_p^* + 2\epsilon_m^*} \tag{3.2}$$

where, ϵ_m^* *and* ϵ_p^* are the complex permittivity of the surrounding medium and the particle, respectively. The sign of the Clausius Mossotti factor determines the direction of the dielectrophoretic force [35].

$$\epsilon(\omega)_i = \epsilon_{i\infty} + \sum \frac{\triangle\epsilon_{in}}{1 + (jw_n\tau_{in})^{\alpha_{in}}} \; where \; n = 1, 2, 3, 4 \tag{3.3}$$

$$\epsilon^*_{i(i=p,m)} = \epsilon(\omega)_i - j\frac{\sigma_i}{\epsilon_0\omega} \tag{3.4}$$

where, σ denotes the conductivity, τ is the relaxation time, ω is the radian frequency, $\triangle\epsilon_n$ is the relative dielectric permittivity between the low and the high frequencies in the $n-th$ dispersion region and $j = \sqrt{-1}$ [35].

4. RESULTS

4.1 Introduction

An adequate blood flow is vital for bone healing [16]. DEPF might be used to step up the velocity of blood flow near the fracture site and thus enhance healing. In order to create the DEPF there must be a sufficiently large non-uniform electric field. To generate this non-uniform field, in the present thesis, we have considered three different coil models; namely, the linear, the parabolic and the square root coil models as shown in Figure 4.1.

4.2 The Coil Model

The coil model considered in this thesis is shown in Figure 4.1. The height, the interwinding distance and the diameter of each turn of the coil are chosen as 28 cm and 0.5 cm and 0.25 cm respectively, after some trial-and-error process. The radius of each turn is different in order to acquire a non-uniform electric field inside the coil. In the center of the coil, the radius of the turn is r1 and at the top, the radius of the turn is r20. The values of the radii are in the increasing order from the center to the top. As seen from Figure 4.1, the coil is symmetric in the z axis so that the lower part of the coil has the same parameters as the upper part.

The derivation of the dielectrophoretic forces are given in Appendix A. The dielectrophoresis has a dispersive behaviour, i.e., it has frequency dependence. Figures 4.2-4.9 show that frequency versus the DEPF/rp graphs for linear, parabolic and square root coils, where rp represents the red blood cell radius. As in Figure 4.2, between 5 Hz and 15 Hz, the DEPF/rp value peaks. In the next sections, the details of the coil models are explained.

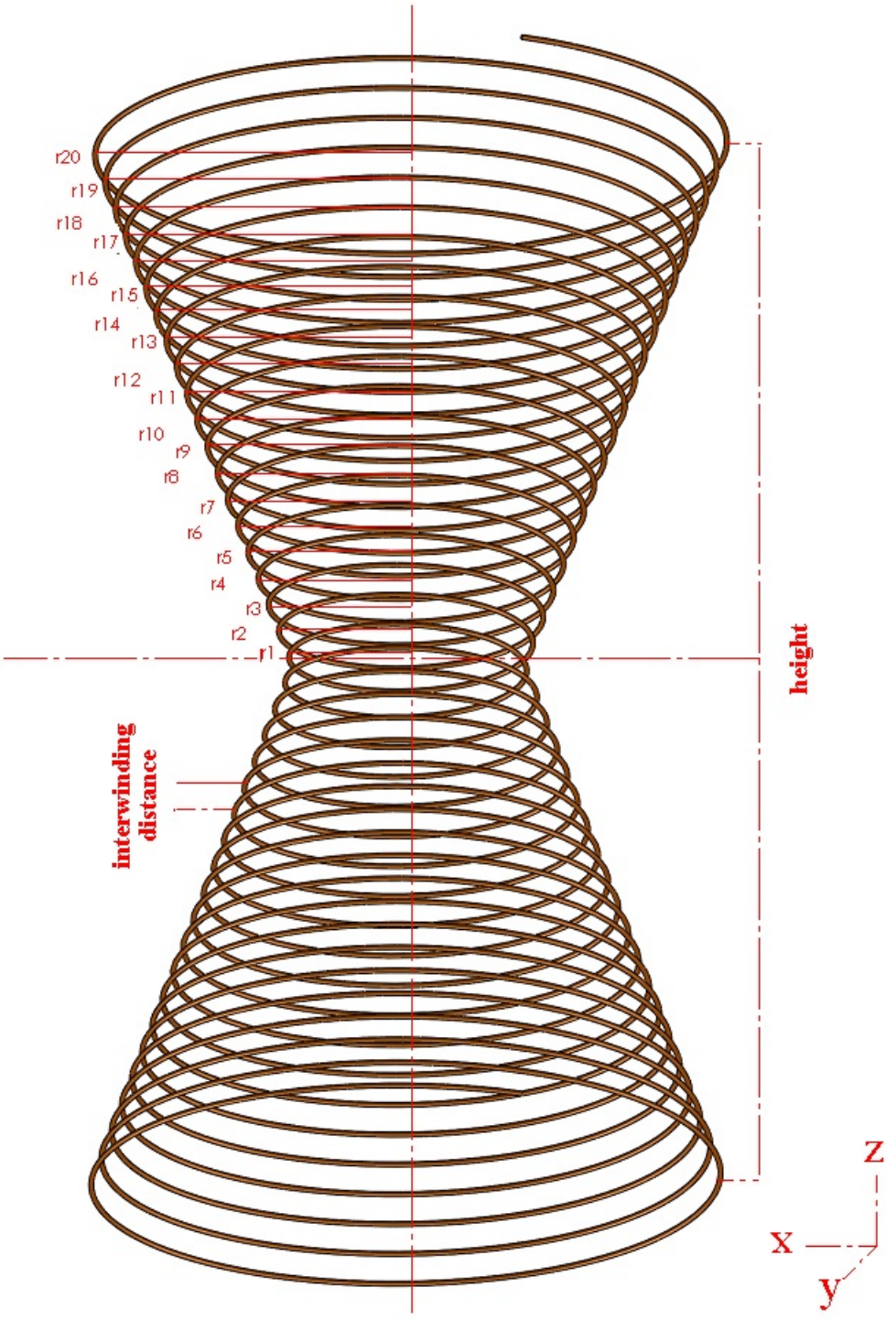

Figure 4.1 Coil model

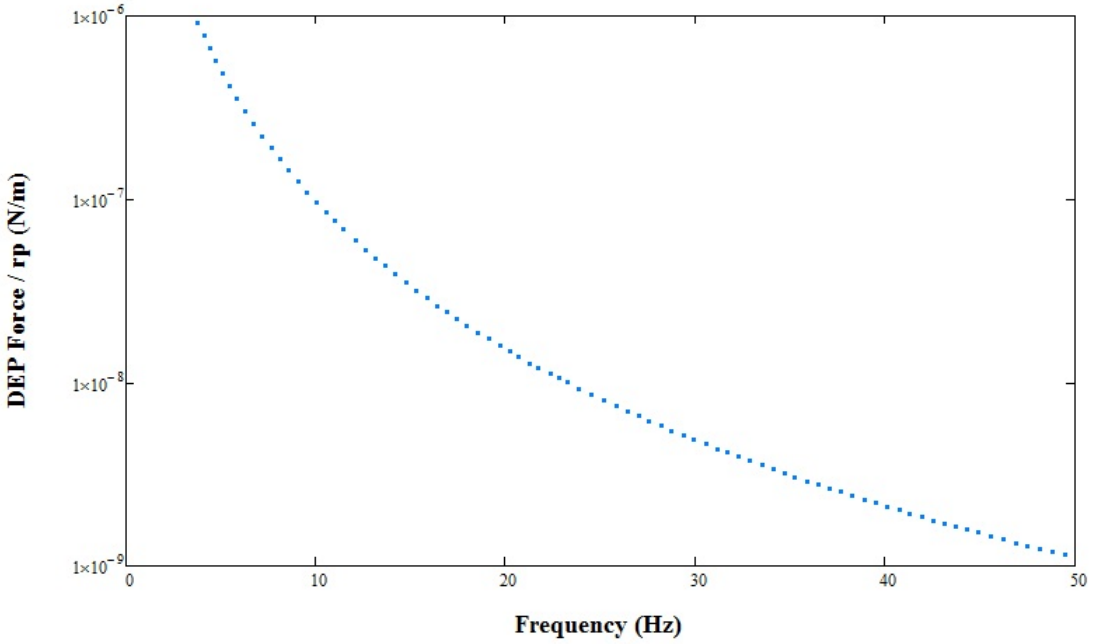

Figure 4.2 The DEPF/rp (N/m) vs frequency (Hz) (0-50 Hz)

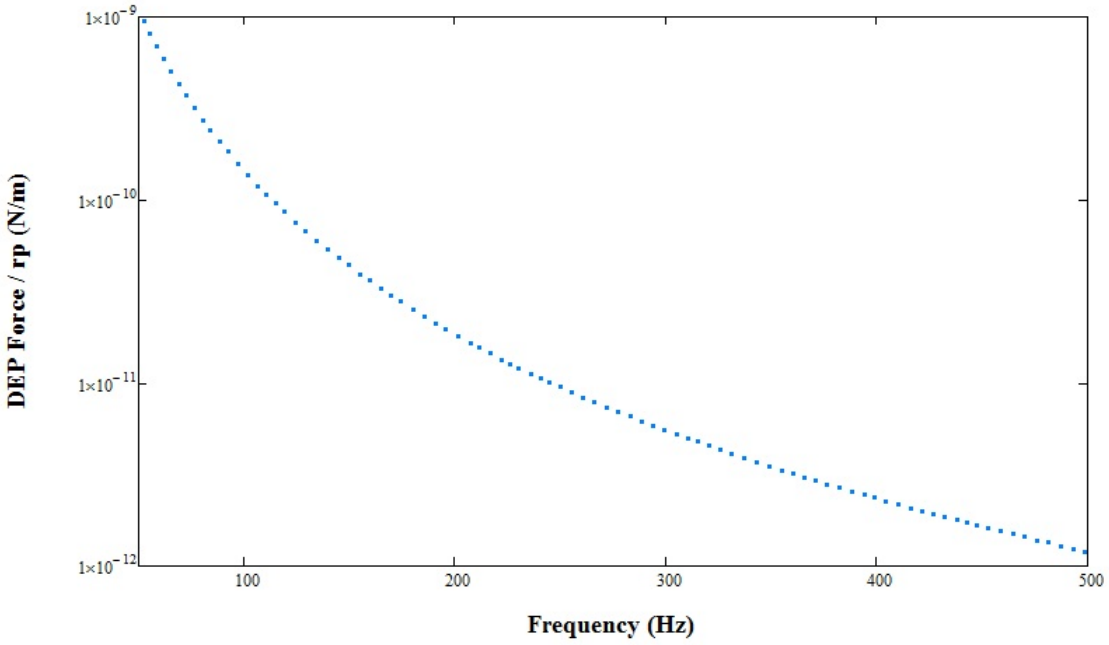

Figure 4.4 The DEPF/rp (N/m) vs frequency (Hz) (50 Hz-500 Hz)

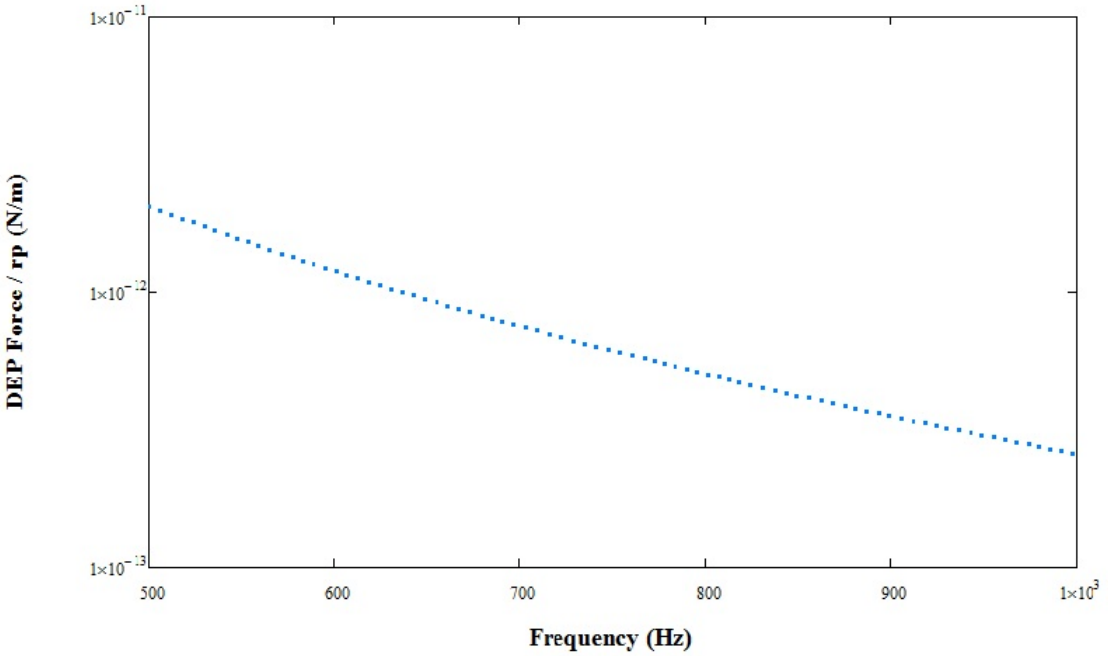

Figure 4.3 The DEPF/rp (N/m) vs frequency (Hz) (500 Hz-1 kHz)

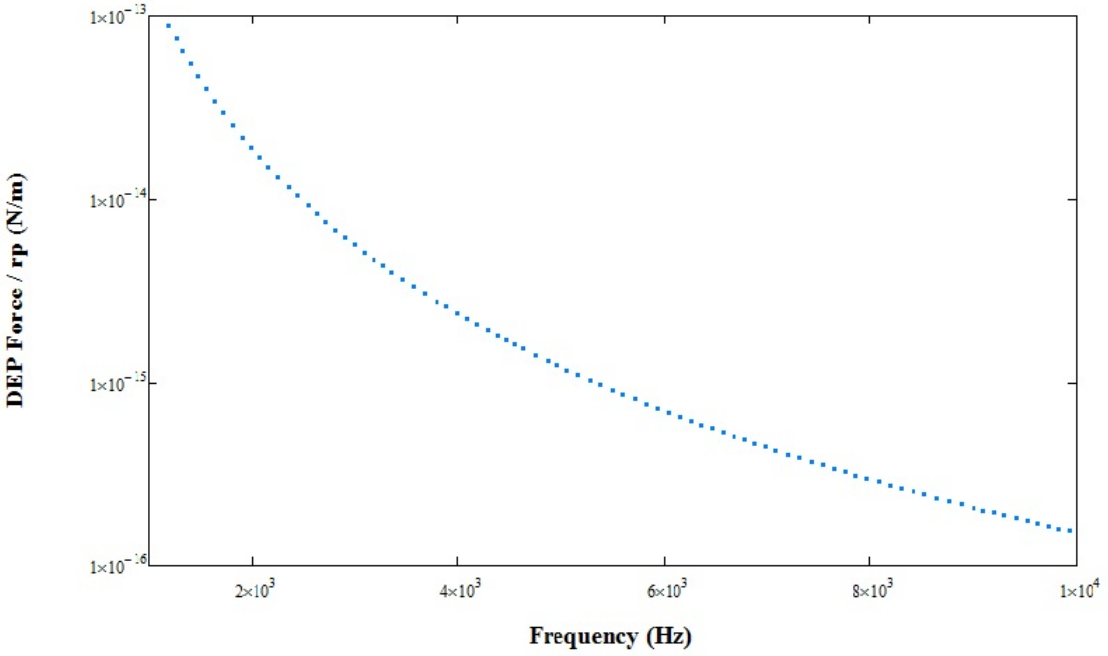

Figure 4.5 The DEPF/rp (N/m) vs frequency (Hz) (1 kHz-10 kHz)

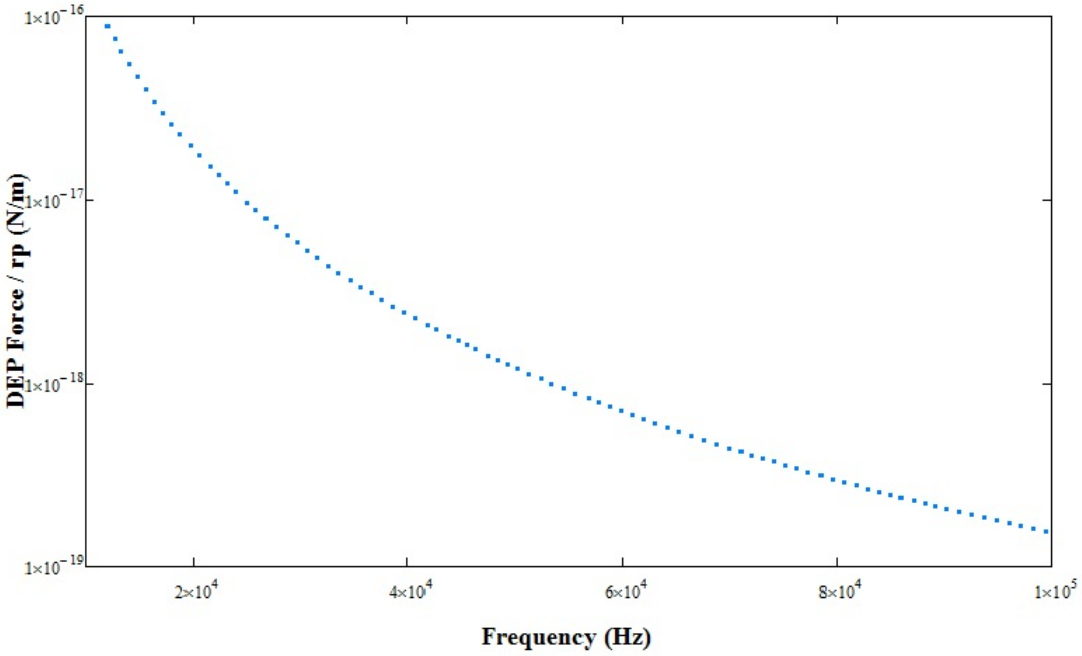

Figure 4.6 The DEPF/rp (N/m) vs frequency (Hz) (10 kHz-100 kHz)

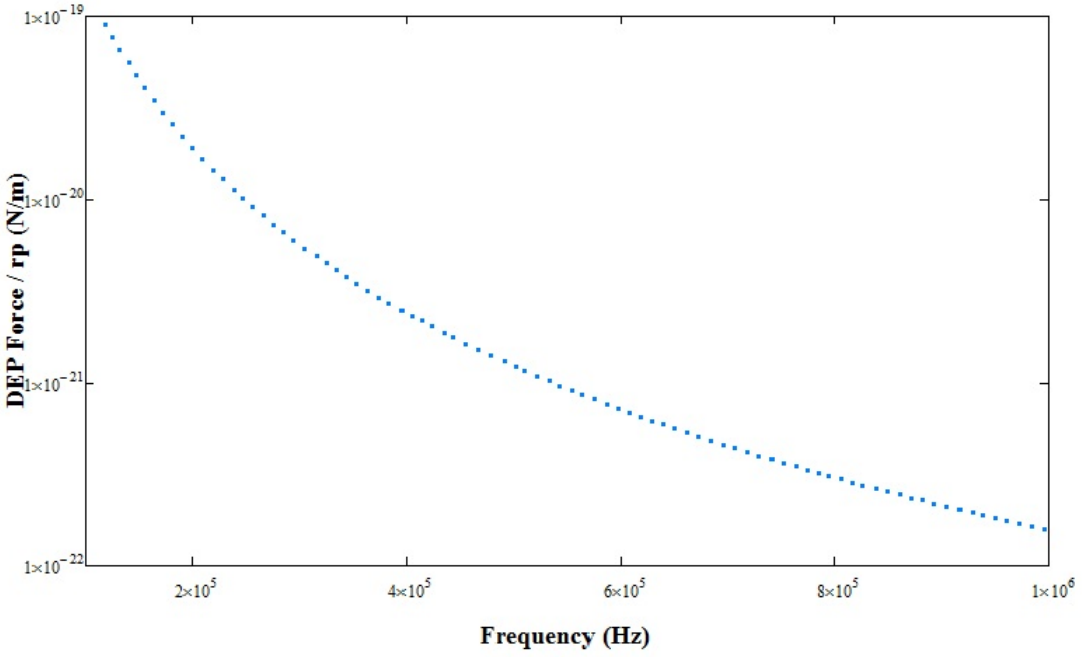

Figure 4.7 The DEPF/rp (N/m) vs frequency (Hz) (100 kHz-1 MHz)

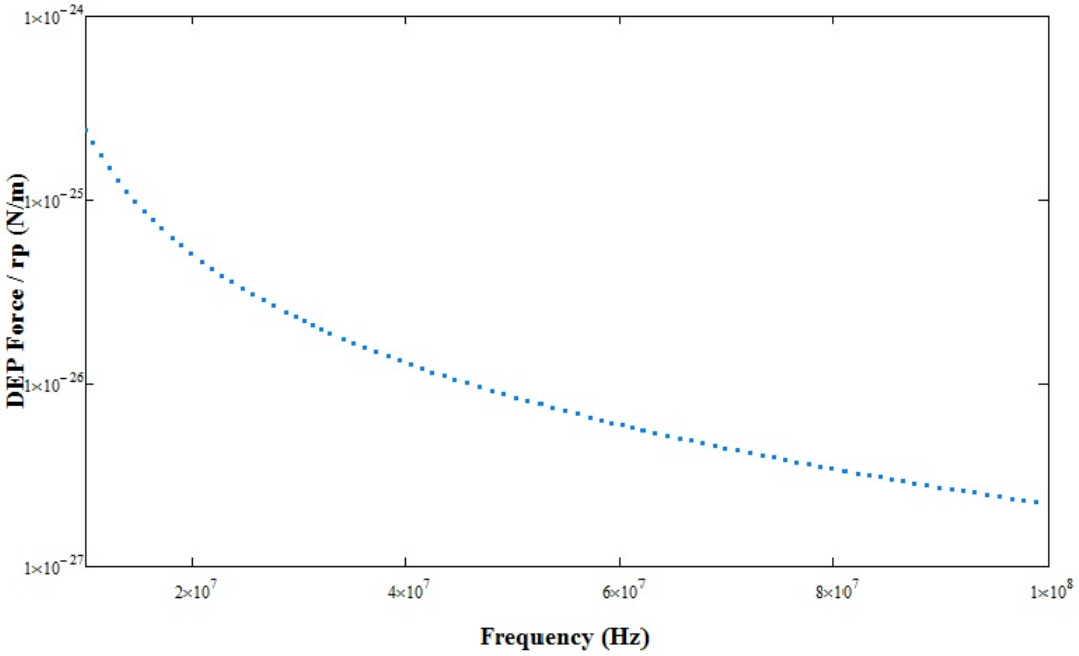

Figure 4.8 The DEPF/rp (N/m) vs frequency (Hz) (10 MHz-100 MHz)

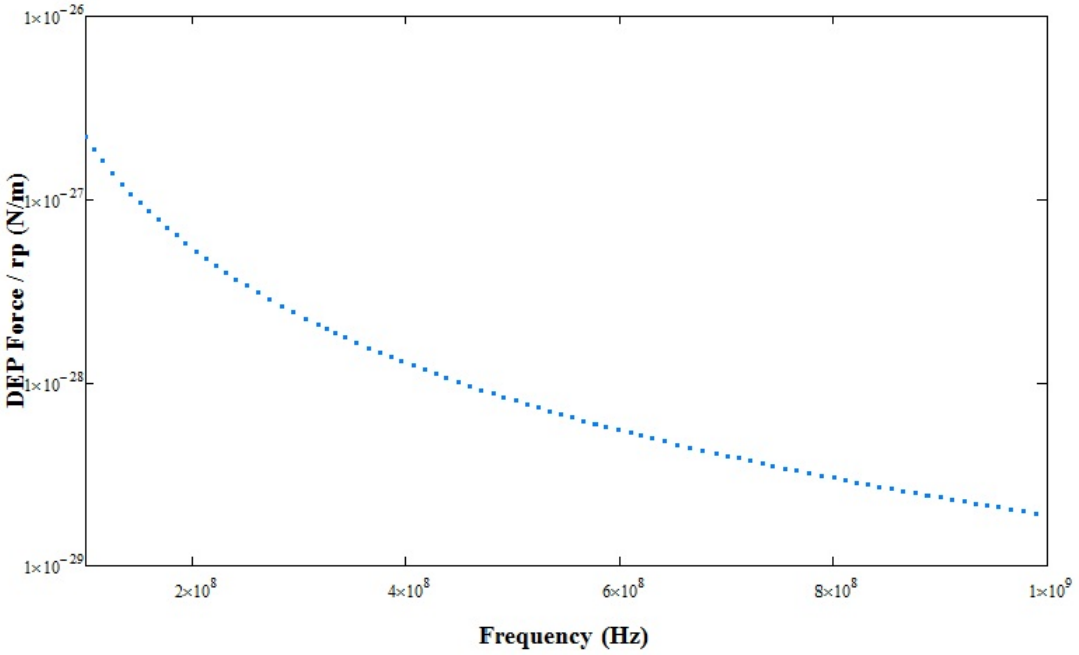

Figure 4.9 The DEPF/rp (N/m) vs frequency (Hz) (100 MHz-1 GHz)

4.3 The Linear, The Parabolic and The Square Root Coils with Distinct Radiuses

In this section, vectorel simulation of dielectrophoretic force and magnetic field intensity for the linear, the parabolic and the square root coil models with different radii are summarized.

4.3.1 The Linear Coil

The equations for the linear coil are $z = x + r1\,cm$ ($r1 = 10, 15, 20\,cm$). In this model, the coil height is 28 cm, the interwinding distance is 0.5 cm. The radii of each turn are calculated for each of the linear coil equation and shown in Tables 4.1-4.3. The DEPF can be calculated for each turn and using superposition the total DEPF can be obtained. The results, for 5 Hz, 10 Hz, 15 Hz are summarized in Tables 4.1-4.3. For all frequencies, the peak value of the DEPF occurs at the center of the coil. When r1=15 cm, for 5 Hz it is $9.73 \times 10^{-8}\ N/m$, for 10 Hz it is $7.43 \times 10^{-8}\ N/m$, for 15 Hz it is $2.55 \times 10^{-8}\ N/m$. These values show that at 5 Hz the DEPF peaks. Tables 4.1-4.3 show that the blood flow rate increases as the center of the coil is approached and in the center the flow peaks.

Since the main arteries follow paths parallel to the tibia and fibula [36], the DEPF is roughly in the same direction as the arteries. In Figure 4.10, a vectorel plot of the DEPF/rp are given along the z and the r axes in cylindrical coordinates. It can be seen that the magnitute of the DEPF/rp diminishes along the z axis. This demonstrates the gradient nature of the linear coil. At the center (z=0) the magnitute peaks as desired. A plot of the magnetic flux intensity versus z is presented in Figure 4.11. The total MFI reaches a peak value of $3.94 \times 10^{-6}\ T$ at z=0 in the center of the coil.

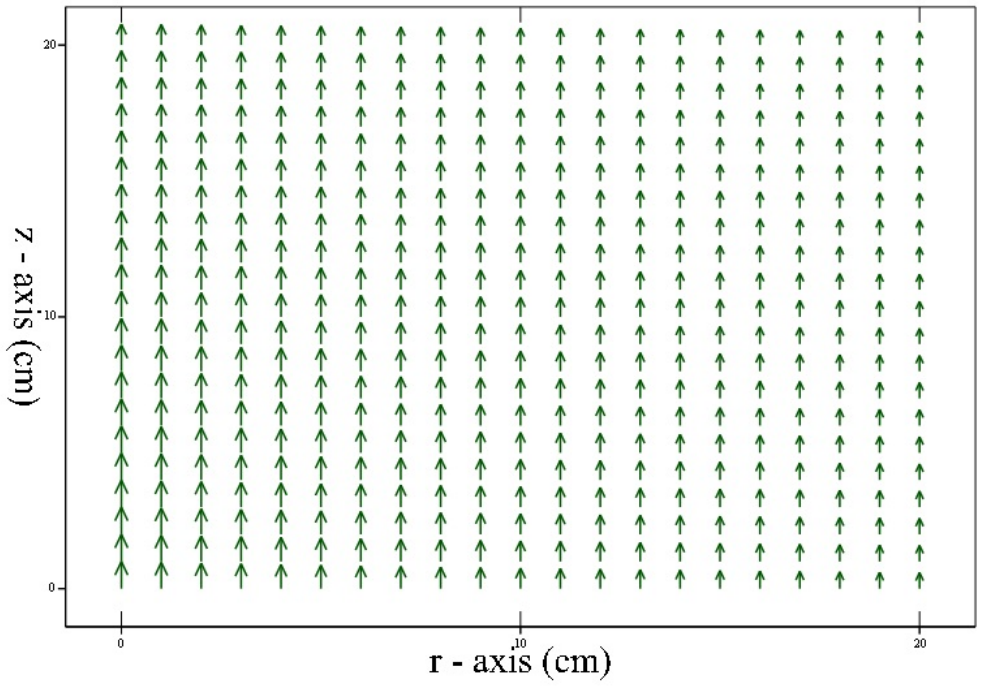

Figure 4.10 The direction of the DEPF/rp inside the linear coil

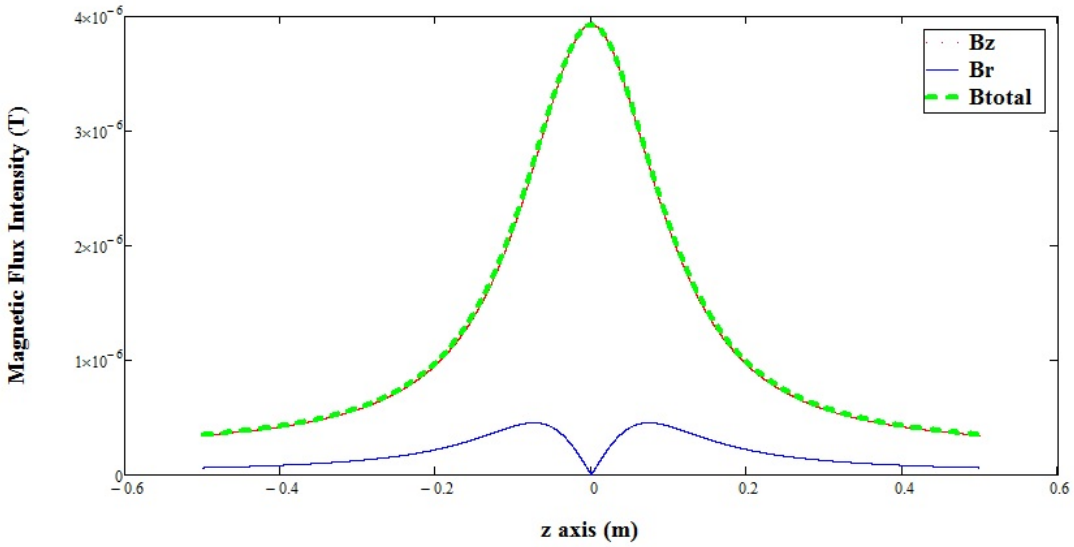

Figure 4.11 Magnetic flux intensity when r1=15 cm

Table 4.1
DEPF/rp Table for The Linear Coil of $z = x + 10\,(cm)$

z-axis (cm)	Radius (cm)	$\frac{DEPF\,(5Hz)}{rp}\ \frac{N}{m}$	$\frac{DEPF\,(10Hz)}{rp}\ \frac{N}{m}$	$\frac{DEPF\,(15Hz)}{rp}\ \frac{N}{m}$
0	10	2.17×10^{-7}	1.66×10^{-7}	5.70×10^{-8}
0.50	10.50	1.96×10^{-7}	1.50×10^{-7}	5.15×10^{-8}
1.25	11.25	1.64×10^{-7}	1.25×10^{-7}	4.32×10^{-8}
2.00	12.00	1.39×10^{-7}	1.07×10^{-7}	3.67×10^{-8}
2.75	12.75	1.16×10^{-7}	8.87×10^{-8}	3.06×10^{-8}
3.50	13.50	9.90×10^{-8}	7.57×10^{-8}	2.61×10^{-8}
4.25	14.25	8.29×10^{-8}	6.63×10^{-8}	2.18×10^{-8}
5.00	15.00	7.13×10^{-8}	5.45×10^{-8}	1.88×10^{-8}
5.75	15.75	6.05×10^{-8}	4.41×10^{-8}	1.59×10^{-8}
6.50	16.50	5.26×10^{-8}	4.02×10^{-8}	1.38×10^{-8}
7.25	17.25	4.52×10^{-8}	3.45×10^{-8}	1.19×10^{-8}
8.00	18.00	3.96×10^{-8}	3.03×10^{-8}	1.05×10^{-8}
8.75	18.75	3.46×10^{-8}	2.64×10^{-8}	9.09×10^{-9}
9.50	19.50	3.07×10^{-8}	2.35×10^{-8}	8.08×10^{-9}
10.25	20.25	2.70×10^{-8}	2.06×10^{-8}	7.11×10^{-9}
11.00	21.00	2.43×10^{-8}	1.85×10^{-8}	6.39×10^{-9}
11.75	21.75	2.16×10^{-8}	1.65×10^{-8}	5.67×10^{-9}
12.50	22.50	1.96×10^{-8}	1.49×10^{-8}	5.14×10^{-9}
13.25	23.25	1.75×10^{-8}	1.34×10^{-8}	4.61×10^{-9}
14.00	24.00	1.60×10^{-8}	1.22×10^{-8}	4.21×10^{-9}

Table 4.2
DEPF/rp Table for The Linear Coil of $z = x + 15\,(cm)$

z-axis (cm)	Radius (cm)	$\frac{DEPF\,(5Hz)}{rp}\ \frac{N}{m}$	$\frac{DEPF\,(10Hz)}{rp}\ \frac{N}{m}$	$\frac{DEPF\,(15Hz)}{rp}\ \frac{N}{m}$
0	15	9.73×10^{-8}	7.43×10^{-8}	2.55×10^{-8}
0.50	15.50	9.09×10^{-8}	6.94×10^{-8}	2.39×10^{-8}
1.25	16.25	8.10×10^{-8}	6.19×10^{-8}	2.13×10^{-8}
2.00	17.00	7.29×10^{-8}	5.67×10^{-8}	1.92×10^{-8}
2.75	17.75	6.65×10^{-8}	4.92×10^{-8}	1.70×10^{-8}
3.50	18.50	5.78×10^{-8}	4.42×10^{-8}	1.52×10^{-8}
4.25	19.25	5.11×10^{-8}	3.91×10^{-8}	1.34×10^{-8}
5.00	20.00	4.59×10^{-8}	3.50×10^{-8}	1.21×10^{-8}
5.75	20.75	4.07×10^{-8}	3.11×10^{-8}	1.07×10^{-8}
6.50	21.50	3.67×10^{-8}	2.81×10^{-8}	9.66×10^{-9}
7.25	22.25	3.27×10^{-8}	2.50×10^{-8}	8.61×10^{-9}
8.00	23.00	2.97×10^{-8}	2.16×10^{-8}	7.80×10^{-9}
8.75	23.75	2.66×10^{-8}	2.03×10^{-8}	6.99×10^{-9}
9.50	24.50	2.42×10^{-8}	1.85×10^{-8}	6.36×10^{-9}
10.25	25.25	2.18×10^{-8}	1.67×10^{-8}	5.74×10^{-9}
11.00	26.00	1.99×10^{-8}	1.53×10^{-8}	5.26×10^{-9}
11.75	26.75	1.81×10^{-8}	1.38×10^{-8}	4.76×10^{-9}
12.50	25.50	1.66×10^{-8}	1.27×10^{-8}	4.38×10^{-9}
13.25	28.25	1.52×10^{-8}	1.16×10^{-8}	4.00×10^{-9}
14.00	29.00	1.41×10^{-8}	1.07×10^{-8}	3.69×10^{-9}

Table 4.3
DEPF/rp Table for The Linear Coil of $z = x + 20\,(cm)$

z-axis (cm)	Radius (cm)	$\frac{DEPF\,(5Hz)}{rp}\ \frac{N}{m}$	$\frac{DEPF\,(10Hz)}{rp}\ \frac{N}{m}$	$\frac{DEPF\,(15Hz)}{rp}\ \frac{N}{m}$
0	20	5.49×10^{-8}	4.19×10^{-8}	1.44×10^{-8}
0.50	20.50	5.22×10^{-8}	2.29×10^{-8}	1.37×10^{-8}
1.25	21.25	4.79×10^{-8}	1.70×10^{-8}	1.26×10^{-8}
2.00	22.00	1.88×10^{-8}	1.43×10^{-8}	1.16×10^{-8}
2.75	22.75	1.61×10^{-8}	1.23×10^{-8}	1.06×10^{-8}
3.50	23.50	1.44×10^{-8}	1.10×10^{-8}	9.82×10^{-9}
4.25	24.25	1.29×10^{-8}	9.85×10^{-9}	8.96×10^{-9}
5.00	25.00	1.18×10^{-8}	9.00×10^{-9}	8.26×10^{-9}
5.75	25.75	1.08×10^{-8}	8.26×10^{-9}	7.52×10^{-9}
6.50	26.50	1.00×10^{-8}	7.69×10^{-9}	6.94×10^{-9}
7.25	27.25	9.33×10^{-9}	7.12×10^{-9}	6.33×10^{-9}
8.00	28.00	8.76×10^{-9}	6.69×10^{-9}	5.86×10^{-9}
8.75	28.75	8.18×10^{-9}	6.25×10^{-9}	5.37×10^{-9}
9.50	29.50	7.74×10^{-9}	5.91×10^{-9}	4.97×10^{-9}
10.25	30.25	7.28×10^{-9}	5.56×10^{-9}	4.56×10^{-9}
11.00	31.00	6.91×10^{-9}	5.28×10^{-9}	4.25×10^{-9}
11.75	31.75	6.53×10^{-9}	4.99×10^{-9}	3.91×10^{-9}
12.50	32.50	6.23×10^{-9}	4.76×10^{-9}	3.64×10^{-9}
13.25	33.25	5.91×10^{-9}	4.52×10^{-9}	3.37×10^{-9}
14.00	34.00	5.65×10^{-9}	4.32×10^{-9}	3.15×10^{-9}

4.3.2 The Parabolic Coil

The equations for the parabolic coil are $z = 0.1x^2 + r1\,cm$ $(r1 = 10, 15, 20\,cm)$. In this model, the coil height is 28 cm, the interwinding distance is 0.5 cm. The radii of each turn are calculated for each of the parabolic coil equation and shown in Tables 4.4-4.6. The DEPF can be calculated for each turn and using superposition the total DEPF can be obtained. The results, for 5 Hz, 10 Hz, 15 Hz are summarized in Tables 4.4-4.6. For all frequencies, the peak value of the DEPF occurs at the center of the coil. When r1=10 cm, for 5 Hz it is $2.17 \times 10^{-7}\ N/m$, for 10 Hz it is $1.66 \times 10^{-7}\ N/m$, for 15 Hz it is $5.70 \times 10^{-8}\ N/m$. These values show that at 5 Hz the DEPF peaks. Tables 4.4-4.6 show that the blood flow rate increases as the center of the coil is approached and in the center the flow peaks.

Since the main arteries follow paths parallel to the tibia and fibula [36], the DEPF is roughly in the same direction as the arteries. In Figure 4.12, a vectorel plot of the DEPF/rp are given along the z and the r axes in cylindrical coordinates. It can be seen that the magnitute of the DEPF/rp diminishes along the z axis. This demonstrates the gradient nature of the parabolic coil. At the center (z=0) the magnitute peaks as desired. A plot of the magnetic flux intensity versus z is presented in Figure 4.13. The total MFI reaches a peak value of $6.13 \times 10^{-6}\ T$ at z=0 in the center of the coil.

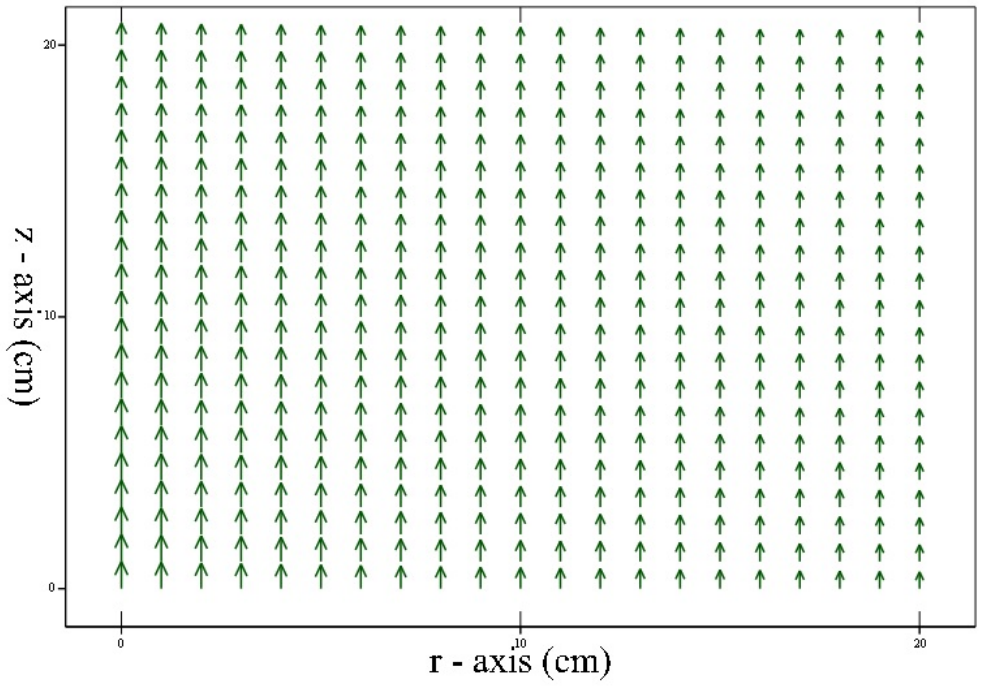

Figure 4.12 The direction of the DEPF/rp inside the parabolic coil

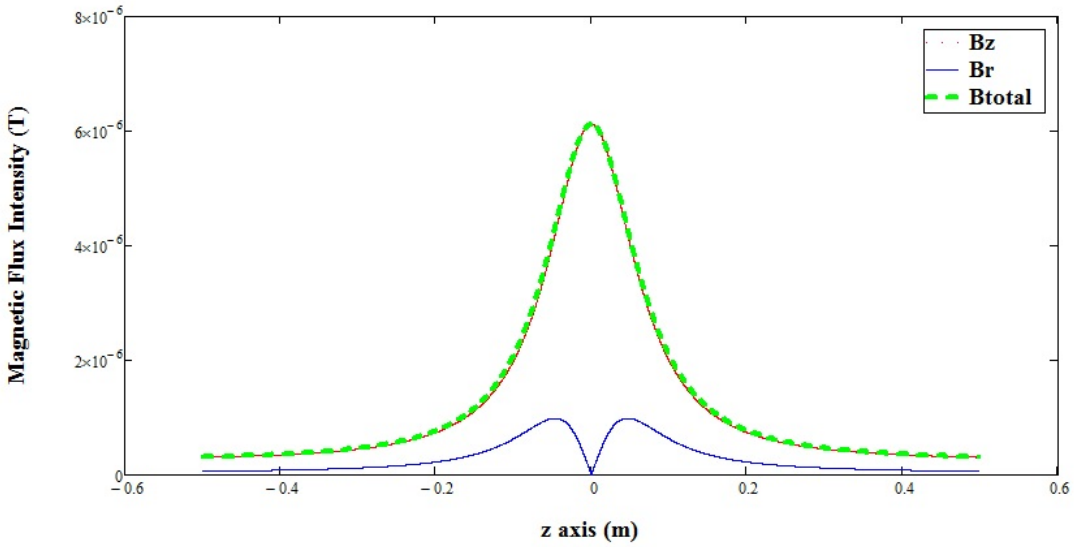

Figure 4.13 Magnetic flux intensity when r1=10 cm

Table 4.4
DEPF/rp Table for The Parabolic Coil of $z = 0.1x^2 + 10\,(cm)$

z-axis (cm)	Radius (cm)	$\frac{DEPF\,(5Hz)}{rp}\ \frac{N}{m}$	$\frac{DEPF\,(10Hz)}{rp}\ \frac{N}{m}$	$\frac{DEPF\,(15Hz)}{rp}\ \frac{N}{m}$
0	10	2.17×10^{-7}	1.66×10^{-7}	5.70×10^{-8}
0.50	10.03	2.15×10^{-7}	1.63×10^{-7}	5.66×10^{-8}
1.25	10.16	2.06×10^{-7}	1.57×10^{-7}	5.42×10^{-8}
2.00	10.40	1.92×10^{-7}	1.46×10^{-7}	5.06×10^{-8}
2.75	10.76	1.72×10^{-7}	1.31×10^{-7}	4.53×10^{-8}
3.50	11.22	1.53×10^{-7}	1.16×10^{-7}	4.01×10^{-8}
4.25	11.81	1.29×10^{-7}	9.90×10^{-8}	3.41×10^{-8}
5.00	12.50	1.10×10^{-7}	8.46×10^{-8}	2.91×10^{-8}
5.75	13.31	9.12×10^{-8}	6.90×10^{-8}	2.39×10^{-8}
6.50	14.22	7.63×10^{-8}	5.82×10^{-8}	2.00×10^{-8}
7.25	15.26	6.19×10^{-8}	4.72×10^{-8}	1.62×10^{-8}
8.00	16.40	5.14×10^{-8}	3.92×10^{-8}	1.35×10^{-8}
8.75	17.66	4.56×10^{-8}	3.17×10^{-8}	1.09×10^{-8}
9.50	19.03	3.46×10^{-8}	2.64×10^{-8}	9.09×10^{-9}
10.25	20.50	2.82×10^{-8}	2.15×10^{-8}	7.40×10^{-9}
11.00	22.10	2.36×10^{-8}	1.80×10^{-8}	6.21×10^{-9}
11.75	23.81	1.94×10^{-8}	1.49×10^{-8}	5.11×10^{-9}
12.50	25.63	1.64×10^{-8}	1.31×10^{-8}	4.33×10^{-9}
13.25	27.56	1.37×10^{-8}	1.05×10^{-8}	3.62×10^{-9}
14.00	29.60	1.18×10^{-8}	9.03×10^{-9}	3.11×10^{-9}

Table 4.5
DEPF/rp Table for The Parabolic Coil of $z = 0.1x^2 + 15\,(cm)$

z-axis (cm)	Radius (cm)	$\frac{DEPF\,(5Hz)}{rp}\ \frac{N}{m}$	$\frac{DEPF\,(10Hz)}{rp}\ \frac{N}{m}$	$\frac{DEPF\,(15Hz)}{rp}\ \frac{N}{m}$
0	15	9.73×10^{-8}	7.43×10^{-8}	2.55×10^{-8}
0.50	15.03	9.69×10^{-8}	7.40×10^{-8}	2.50×10^{-8}
1.25	15.16	9.50×10^{-8}	7.25×10^{-8}	2.43×10^{-8}
2.00	15.40	9.19×10^{-8}	7.02×10^{-8}	2.40×10^{-8}
2.75	15.76	8.72×10^{-8}	6.65×10^{-8}	2.29×10^{-8}
3.50	16.22	8.21×10^{-8}	6.27×10^{-8}	2.16×10^{-8}
4.25	16.81	7.57×10^{-8}	5.78×10^{-8}	1.99×10^{-8}
5.00	17.50	6.97×10^{-8}	5.32×10^{-8}	1.83×10^{-8}
5.75	18.31	6.27×10^{-8}	4.78×10^{-8}	1.65×10^{-8}
6.50	19.22	5.69×10^{-8}	4.34×10^{-8}	1.49×10^{-8}
7.25	20.26	5.04×10^{-8}	3.84×10^{-8}	1.32×10^{-8}
8.00	21.40	4.50×10^{-8}	3.44×10^{-8}	1.18×10^{-8}
8.75	22.66	3.95×10^{-8}	3.02×10^{-8}	1.03×10^{-8}
9.50	24.03	3.50×10^{-8}	2.68×10^{-8}	9.20×10^{-9}
10.25	25.50	3.06×10^{-8}	2.34×10^{-8}	8.05×10^{-9}
11.00	27.10	2.71×10^{-8}	2.07×10^{-8}	7.05×10^{-9}
11.75	28.81	2.36×10^{-8}	1.81×10^{-8}	6.22×10^{-9}
12.50	30.63	2.10×10^{-8}	1.60×10^{-8}	5.52×10^{-9}
13.25	32.56	1.83×10^{-8}	1.40×10^{-8}	4.82×10^{-9}
14.00	34.60	1.63×10^{-8}	1.25×10^{-8}	4.29×10^{-9}

Table 4.6
DEPF/rp Table for The Parabolic Coil of $z = 0.1x^2 + 20\,(cm)$

z-axis (cm)	Radius (cm)	$\frac{DEPF\,(5Hz)}{rp}\ \frac{N}{m}$	$\frac{DEPF\,(10Hz)}{rp}\ \frac{N}{m}$	$\frac{DEPF\,(15Hz)}{rp}\ \frac{N}{m}$
0	20	5.49×10^{-8}	4.19×10^{-8}	1.44×10^{-8}
0.50	20.03	5.48×10^{-8}	4.18×10^{-8}	1.42×10^{-8}
1.25	20.16	5.42×10^{-8}	4.13×10^{-8}	1.41×10^{-8}
2.00	20.40	5.31×10^{-8}	4.06×10^{-8}	1.39×10^{-8}
2.75	20.76	5.15×10^{-8}	3.93×10^{-8}	1.35×10^{-8}
3.50	21.22	4.97×10^{-8}	3.79×10^{-8}	1.32×10^{-8}
4.25	21.81	4.73×10^{-8}	3.61×10^{-9}	1.26×10^{-8}
5.00	23.50	4.50×10^{-8}	3.44×10^{-8}	1.20×10^{-8}
5.75	24.31	4.21×10^{-8}	3.22×10^{-8}	1.13×10^{-8}
6.50	24.22	3.96×10^{-8}	3.02×10^{-8}	1.07×10^{-8}
7.25	25.26	3.66×10^{-8}	2.80×10^{-8}	9.94×10^{-9}
8.00	26.40	3.41×10^{-8}	2.60×10^{-8}	9.27×10^{-9}
8.75	27.66	3.12×10^{-8}	2.38×10^{-8}	8.52×10^{-9}
9.50	29.03	2.89×10^{-8}	2.20×10^{-8}	7.87×10^{-9}
10.25	30.50	2.63×10^{-8}	2.00×10^{-8}	7.16×10^{-9}
11.00	32.10	2.41×10^{-8}	1.84×10^{-8}	6.57×10^{-9}
11.75	33.81	2.19×10^{-8}	1.66×10^{-8}	5.93×10^{-9}
12.50	35.63	2.00×10^{-8}	1.54×10^{-8}	5.41×10^{-9}
13.25	37.56	1.80×10^{-8}	1.38×10^{-8}	4.86×10^{-9}
14.00	39.60	1.65×10^{-8}	1.26×10^{-8}	4.41×10^{-9}

4.3.3 The Square Root Coil

The equations for the square root coil are $z = \sqrt{x} + r1\,cm$ $(r1 = 10, 15, 20\,cm)$. In this model, the coil height is 28 cm, the interwinding distance is 0.5 cm. The radii of each turn are calculated for each of the square root coil equation and shown in Tables 4.7-4.9. The DEPF can be calculated for each turn and using superposition the total DEPF can be obtained. The results, for 5 Hz, 10 Hz, 15 Hz are summarized in Tables 4.7-4.9. For all frequencies, the peak value of the DEPF occurs at the center of the coil. When r1=20 cm, for 5 Hz it is $5.49 \times 10^{-8}\ N/m$, for 10 Hz it is $4.19 \times 10^{-8}\ N/m$, for 15 Hz it is $1.44 \times 10^{-8}\ N/m$. These values show that at 5 Hz the DEPF peaks. Tables 4.7-4.9 show that the blood flow rate increases as the center of the coil is approached and in the center the flow peaks.

Since the main arteries follow paths parallel to the tibia and fibula [36], the DEPF is roughly in the same direction as the arteries. In Figure 4.14, a vectorel plot of the DEPF/rp are given along the z and the r axes in cylindrical coordinates. It can be seen that the magnitute of the DEPF/rp diminishes along the z axis. This demonstrates the gradient nature of the square root coil. At the center (z=0) the magnitute peaks as desired. A plot of the magnetic flux intensity versus z is presented in Figure 4.15. The total MFI reaches a peak value of $2.91 \times 10^{-6}\ T$ at z=0 in the center of the coil.

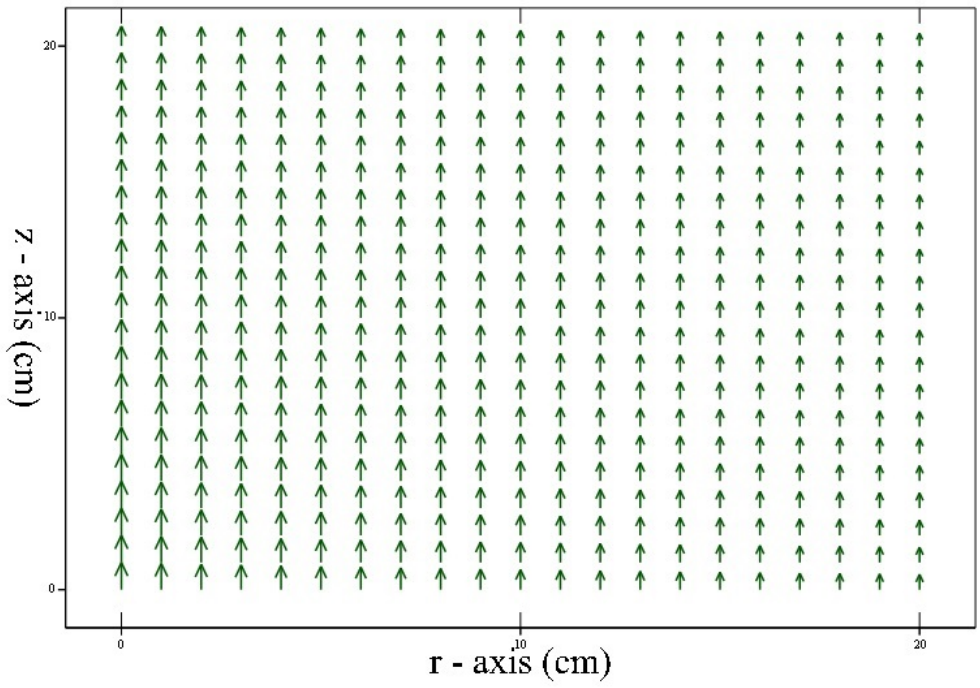

Figure 4.14 The direction of the DEPF/rp inside the square root coil

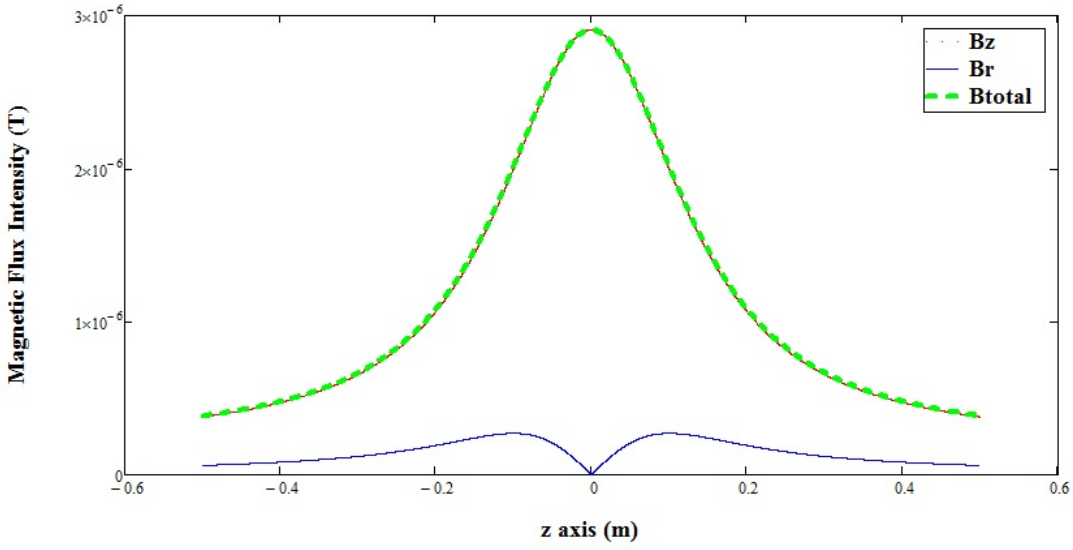

Figure 4.15 Magnetic flux intensity when r1=20 cm

Table 4.7
DEPF/rp Table for The Square Root Coil. $z = \sqrt{x} + 10\,(cm)$

z-axis (cm)	Radius (cm)	$\frac{DEPF\,(5Hz)}{rp}\ \frac{N}{m}$	$\frac{DEPF\,(10Hz)}{rp}\ \frac{N}{m}$	$\frac{DEPF\,(15Hz)}{rp}\ \frac{N}{m}$
0	10	2.17×10^{-7}	1.66×10^{-7}	5.70×10^{-8}
0.50	10.71	7.51×10^{-8}	5.73×10^{-8}	4.98×10^{-8}
1.25	11.12	4.75×10^{-8}	3.63×10^{-8}	4.02×10^{-8}
2.00	11.41	3.70×10^{-8}	2.82×10^{-8}	3.54×10^{-8}
2.75	11.66	2.99×10^{-8}	2.28×10^{-8}	2.97×10^{-8}
3.50	11.87	2.56×10^{-8}	1.96×10^{-8}	2.50×10^{-8}
4.25	12.06	2.21×10^{-8}	1.69×10^{-8}	2.11×10^{-8}
5.00	12.24	1.97×10^{-8}	1.50×10^{-8}	1.81×10^{-8}
5.75	12.40	1.75×10^{-8}	1.33×10^{-8}	1.60×10^{-8}
6.50	12.55	1.59×10^{-8}	1.21×10^{-8}	1.23×10^{-8}
7.25	12.70	1.44×10^{-8}	1.10×10^{-8}	1.13×10^{-8}
8.00	12.83	1.32×10^{-8}	1.00×10^{-8}	8.91×10^{-9}
8.75	12.96	1.22×10^{-8}	9.30×10^{-9}	7.64×10^{-9}
9.50	13.08	1.13×10^{-8}	8.66×10^{-9}	6.50×10^{-9}
10.25	13.20	1.05×10^{-8}	8.01×10^{-9}	5.40×10^{-9}
11.00	13.32	9.80×10^{-9}	7.51×10^{-9}	4.53×10^{-9}
11.75	13.43	9.18×10^{-9}	7.00×10^{-9}	3.79×10^{-9}
12.50	13.54	8.65×10^{-9}	6.60×10^{-9}	3.14×10^{-9}
13.25	13.64	8.10×10^{-9}	6.19×10^{-9}	2.58×10^{-9}
14.00	13.74	7.67×10^{-9}	5.86×10^{-9}	1.99×10^{-9}

Table 4.8
DEPF/rp Table for The Square Root Coil of $z = \sqrt{x} + 15\,(cm)$

z-axis (cm)	Radius (cm)	$\frac{DEPF\,(5Hz)}{rp}\ \frac{N}{m}$	$\frac{DEPF\,(10Hz)}{rp}\ \frac{N}{m}$	$\frac{DEPF\,(15Hz)}{rp}\ \frac{N}{m}$
0	15	9.73×10^{-8}	7.43×10^{-8}	2.55×10^{-8}
0.50	15.71	4.50×10^{-8}	3.44×10^{-8}	1.19×10^{-8}
1.25	16.12	3.14×10^{-8}	2.39×10^{-8}	8.25×10^{-9}
2.00	16.41	2.56×10^{-8}	1.96×10^{-8}	6.74×10^{-9}
2.75	16.66	2.14×10^{-8}	1.64×10^{-8}	5.56×10^{-9}
3.50	16.87	1.88×10^{-8}	1.44×10^{-8}	4.95×10^{-9}
4.25	17.06	1.65×10^{-8}	1.27×10^{-8}	4.36×10^{-9}
5.00	17.24	1.50×10^{-8}	1.14×10^{-8}	3.95×10^{-9}
5.75	17.40	1.36×10^{-8}	1.03×10^{-8}	3.57×10^{-9}
6.50	17.55	1.25×10^{-8}	9.55×10^{-9}	3.29×10^{-9}
7.25	17.70	1.15×10^{-8}	8.76×10^{-9}	3.01×10^{-9}
8.00	17.83	1.07×10^{-8}	8.16×10^{-9}	2.81×10^{-9}
8.75	17.96	9.98×10^{-9}	7.56×10^{-9}	2.60×10^{-9}
9.50	18.08	9.30×10^{-9}	7.10×10^{-9}	2.45×10^{-9}
10.25	18.20	8.69×10^{-9}	6.63×10^{-9}	2.28×10^{-9}
11.00	18.32	8.27×10^{-9}	6.26×10^{-9}	2.15×10^{-9}
11.75	18.43	7.70×10^{-9}	5.88×10^{-9}	2.03×10^{-9}
12.50	18.54	7.31×10^{-9}	5.58×10^{-9}	1.92×10^{-9}
13.25	18.64	6.89×10^{-9}	5.26×10^{-9}	1.81×10^{-9}
14.00	18.74	6.56×10^{-9}	5.01×10^{-9}	1.72×10^{-9}

Table 4.9
DEPF/rp Table for The Square Root Coil of $z = \sqrt{x} + 20\,(cm)$

z-axis (cm)	Radius (cm)	$\frac{DEPF\,(5Hz)}{rp}\ \frac{N}{m}$	$\frac{DEPF\,(10Hz)}{rp}\ \frac{N}{m}$	$\frac{DEPF\,(15Hz)}{rp}\ \frac{N}{m}$
0	20	5.49×10^{-8}	4.19×10^{-8}	1.44×10^{-8}
0.50	20.71	3.00×10^{-8}	2.29×10^{-8}	7.90×10^{-9}
1.25	21.12	2.22×10^{-8}	1.70×10^{-8}	5.86×10^{-9}
2.00	21.41	1.88×10^{-8}	1.43×10^{-8}	4.93×10^{-9}
2.75	21.66	1.61×10^{-8}	1.23×10^{-8}	4.24×10^{-9}
3.50	21.87	1.44×10^{-8}	1.10×10^{-8}	3.79×10^{-9}
4.25	22.06	1.29×10^{-8}	9.85×10^{-9}	3.39×10^{-9}
5.00	22.24	1.18×10^{-8}	9.00×10^{-9}	3.11×10^{-9}
5.75	22.40	1.08×10^{-8}	8.26×10^{-9}	2.84×10^{-9}
6.50	22.55	1.00×10^{-8}	7.69×10^{-9}	2.64×10^{-9}
7.25	22.70	9.33×10^{-9}	7.12×10^{-9}	2.45×10^{-9}
8.00	22.83	8.76×10^{-9}	6.69×10^{-9}	2.30×10^{-9}
8.75	22.96	8.18×10^{-9}	6.25×10^{-9}	2.15×10^{-9}
9.50	23.08	7.74×10^{-9}	5.91×10^{-9}	2.03×10^{-9}
10.25	23.20	7.28×10^{-9}	5.56×10^{-9}	1.91×10^{-9}
11.00	23.32	6.91×10^{-9}	5.28×10^{-9}	1.82×10^{-9}
11.75	23.43	6.53×10^{-9}	4.99×10^{-9}	1.72×10^{-9}
12.50	23.54	6.23×10^{-9}	4.76×10^{-9}	1.64×10^{-9}
13.25	23.64	5.91×10^{-9}	4.52×10^{-9}	1.56×10^{-9}
14.00	23.74	5.65×10^{-9}	4.32×10^{-9}	1.49×10^{-9}

4.3.4 The Effect of The Dielectrophoretic Forces on Blood Flow

In this section the effect of the dielectrophoretic forces on blood flow will be discussed. It is assumed that the long bone fracture under consideration have vertical orientations and the blood flow is downward. Figure 4.16 shows that the gravitational force and the drag force on red blood cells determine the steady state blood flow. The dielectrophoretic force, added to the force balance is functional in increasing the blood flow as shown in Figure 4.17.

The gravitational force on red blood cells are given by (after correcting for the plasma buoyancy);

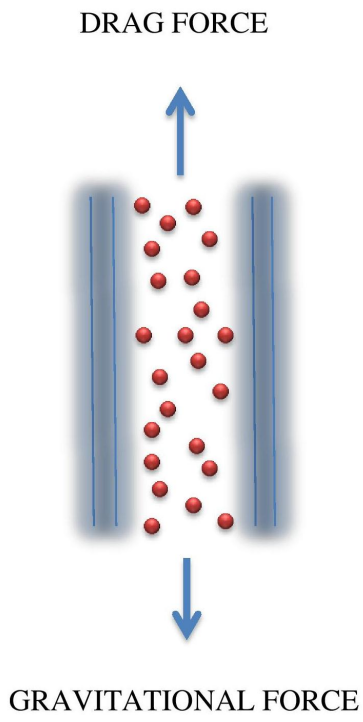

Figure 4.16 Force balance

$$F_{grav} = \frac{4}{3}\pi {r_p}^3 \left(\rho_{rbc} - \rho_{plasma}\right) g \tag{4.1}$$

where, r_p is the radius of the red blood cell, $\rho_{rbc}\ and\ \rho_{plasma}$ are the density of the red blood cell and the blood plasma respectively and g is the acceleration constant [34]. The drag force on the red blood cells are given by:

$$F_{drag} = 6\pi\eta r_p \nu_0 \tag{4.2}$$

where, η is the viscosity of the blood, r_p is the radius of the red blood cell and ν_0 is the velocity (without DEPF) [34]. In the steady state, the force balance equation is:

$$F_{drag} = F_{grav} \tag{4.3}$$

This gives

$$\nu_0 = \frac{2}{9}\frac{\left(\rho_{rbc} - \rho_{plasma}\right)}{\eta} g r_p^2 \tag{4.4}$$

For the red blood cell and the plasma:

$\eta = 0.001\ kg/s,\ \rho_{rbc} = 1100\ kg/m^3\ \rho_{plasma} = 1000\ kg/m^3\ g = 9.81\ m/s^2,\ r_p = 3.84 \times 10^{-6}\ m$ [34].

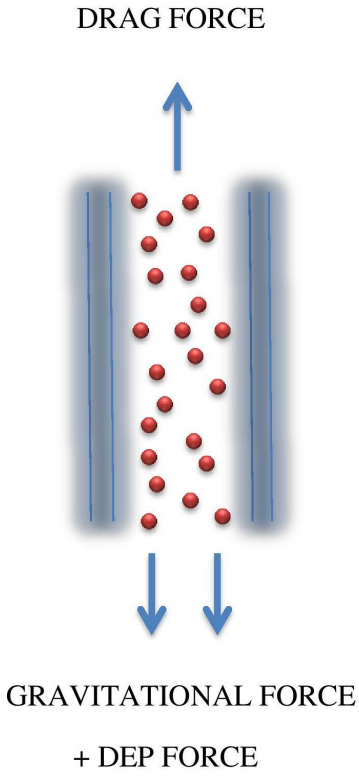

Figure 4.17 New force balance

When there is, in addition, a dielectrophoretic force the above equations will be modified as:

$$F_{drag} = F_{grav} + F_{DEP} \tag{4.5}$$

and the new force balance equation becomes:

$$\nu_{DEPF} = \frac{2}{9}\frac{(\rho_{rbc} - \rho_{plasma})}{\eta} g r_p^2 + \frac{F_{DEP}}{6\pi\eta r_p} \tag{4.6}$$

$$\kappa_{DEPF} = \frac{\nu_{DEPF}}{\nu_0}$$

κ_{DEPF}, the ratio of the velocity in the presence of DEPF to the velocity without DEPF is a good measure of the performance of the DEPF and indicates the increase of blood flow. It will therefore be called the *DEPF factor*.

Figures 4.18-4.26, give a summary of the comparisons of the DEPF/rp vs z values for the linear, the parabolic and the square root coils. As seen from these figures, the peak values of the DEPF/rp are the same for all the coil models. However, the average values are different. Tables 4.10-4.15 show average value of the DEPF/rp and the DEPF factors. Tables 4.16 and 4.17 is a summary of the calculated peak values of the DEPF/rp and the DEPF for the three coil models considered.

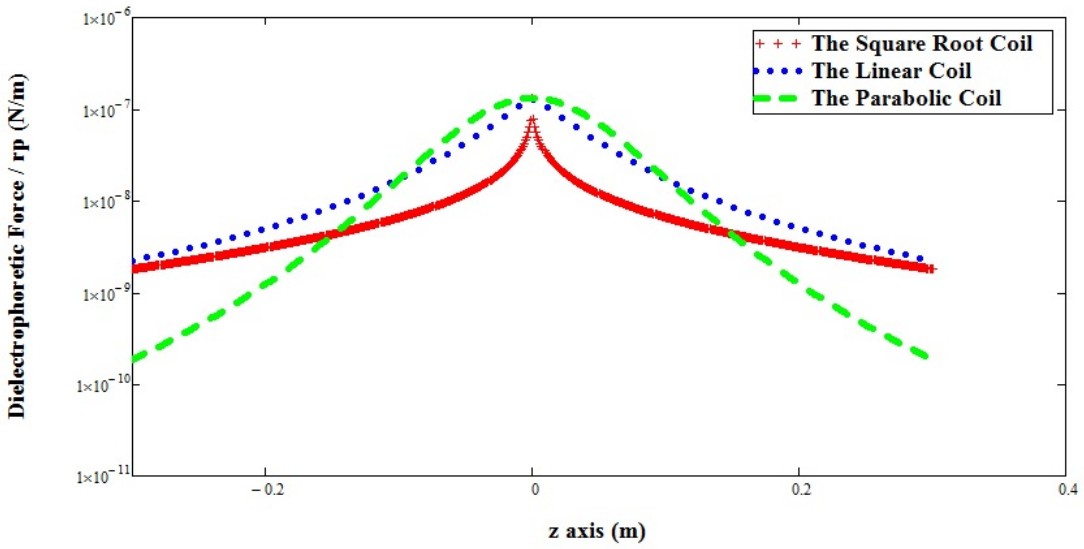

Figure 4.18 Comparison of the linear, the parabolic and the square root coil models (r1=10 cm and f=5 Hz)

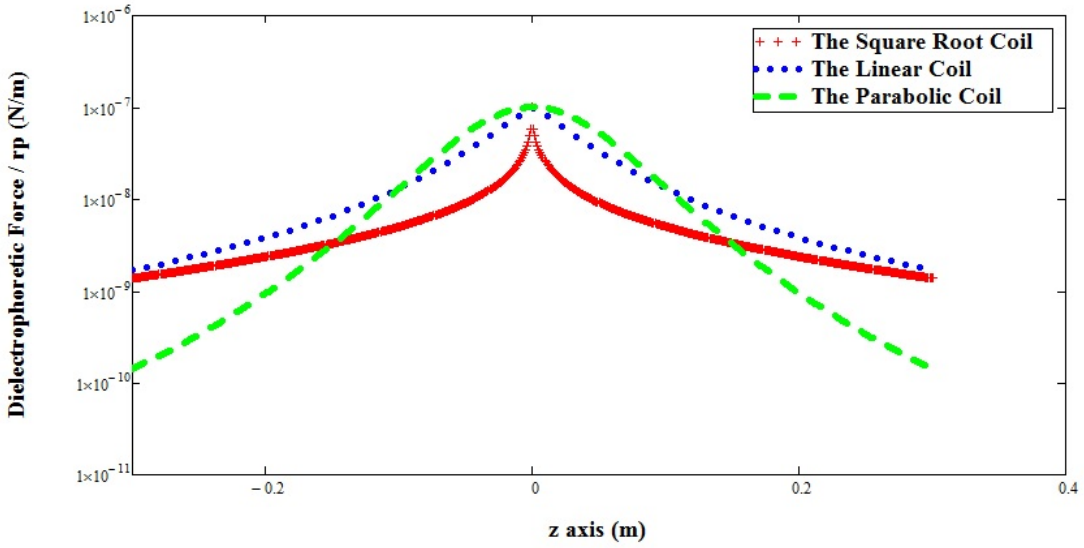

Figure 4.19 Comparison of the linear, the parabolic and the square root coil models (r1=10 cm and f=10 Hz)

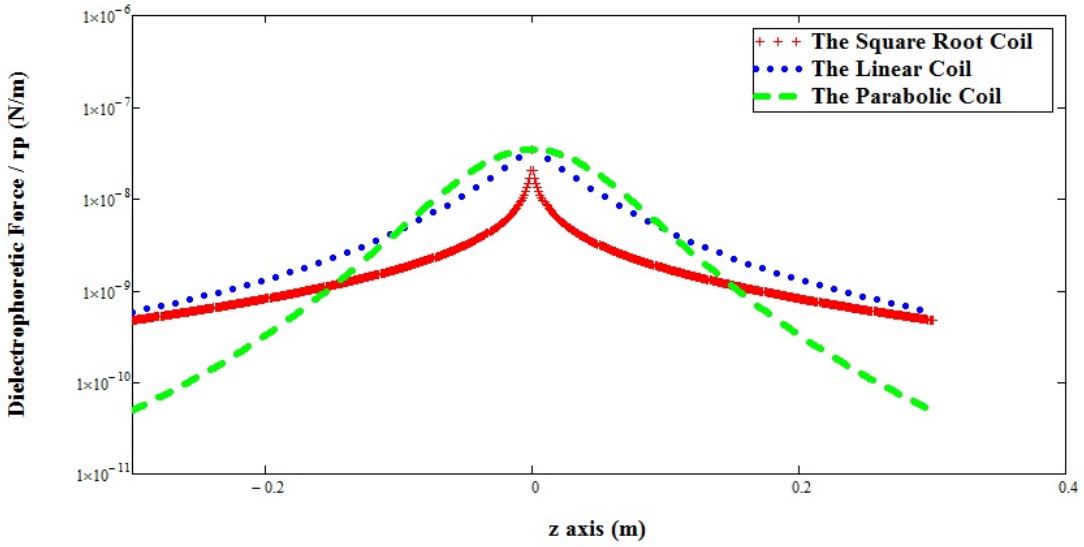

Figure 4.20 Comparison of the linear, the parabolic and the square root coil models (r1=10 cm and f=15 Hz)

Table 4.10
Average Values of The DEPF/rp Inside The Linear, Parabolic and The Square Root Coils (r1=10 cm)

Coil Models	$\frac{DEPF\,(5Hz)}{rp}\ \frac{N}{m}$	$\frac{DEPF\,(10Hz)}{rp}\ \frac{N}{m}$	$\frac{DEPF\,(15Hz)}{rp}\ \frac{N}{m}$
$z = 0.1x^2 + 10\,(cm)$	9.13×10^{-8}	7.02×10^{-8}	2.24×10^{-8}
$z = x + 10\,(cm)$	7.37×10^{-8}	5.63×10^{-8}	1.91×10^{-8}
$z = \sqrt{x} + 10\,(cm)$	3.06×10^{-8}	2.22×10^{-8}	1.80×10^{-8}

Table 4.11
Average Values of The DEPF Factor Inside The Linear, Parabolic and The Square Root Coils (r1=10 cm)

Coil Models	$\kappa_{DEPF}\,(5\,Hz)$	$\kappa_{DEPF}\,(10\,Hz)$	$\kappa_{DEPF}\,(15\,Hz)$
$z = 0.1x^2 + 10\,(cm)$	2.51	2.16	1.37
$z = x + 10\,(cm)$	2.20	1.92	1.31
$z = \sqrt{x} + 10\,(cm)$	1.50	1.36	1.29

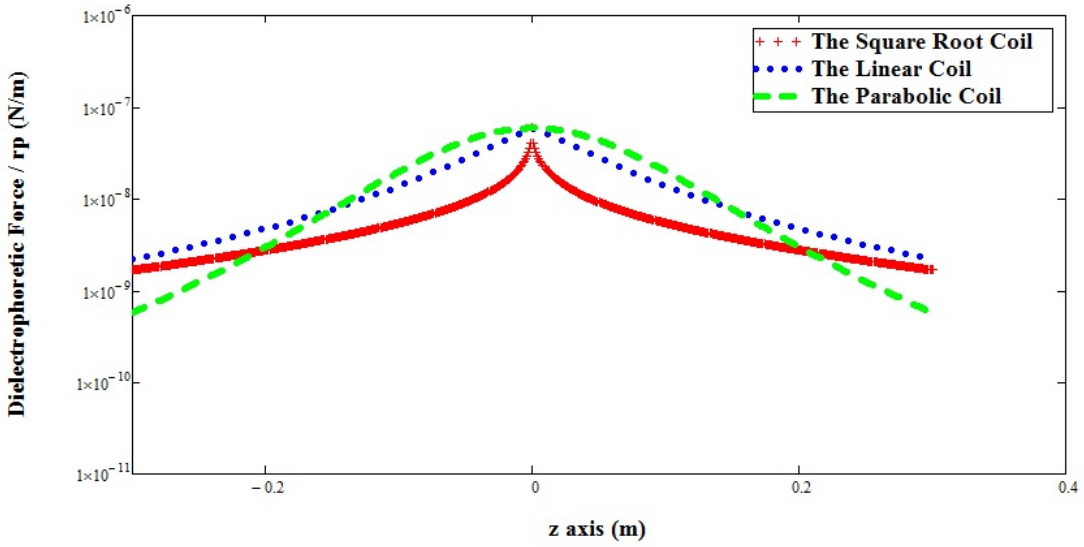

Figure 4.21 Comparison of the linear, the parabolic and the square root coil models (r1=15 cm and f=5 Hz)

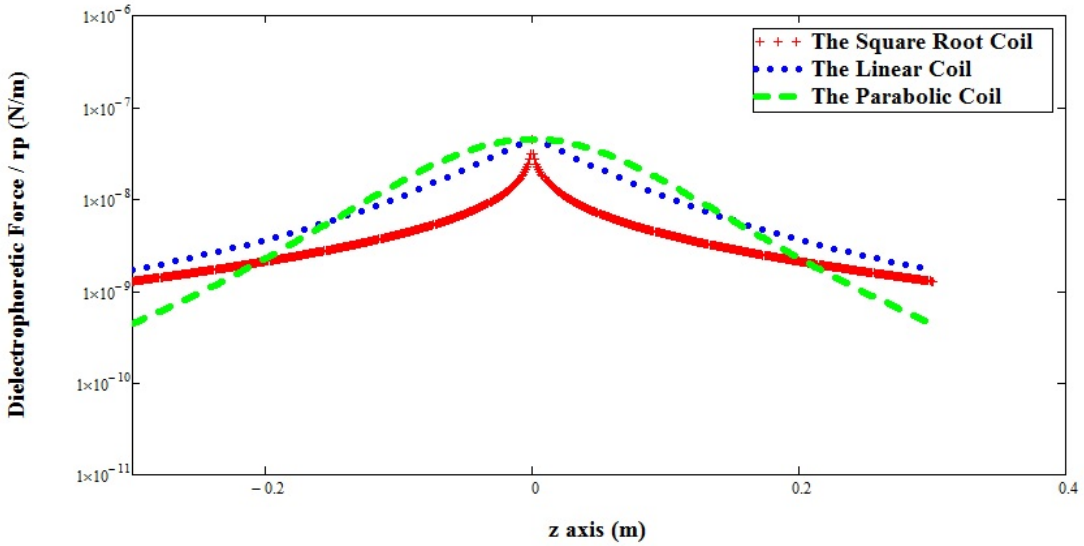

Figure 4.22 Comparison of the linear, the parabolic and the square root coil models (r1=15 cm and f=10 Hz)

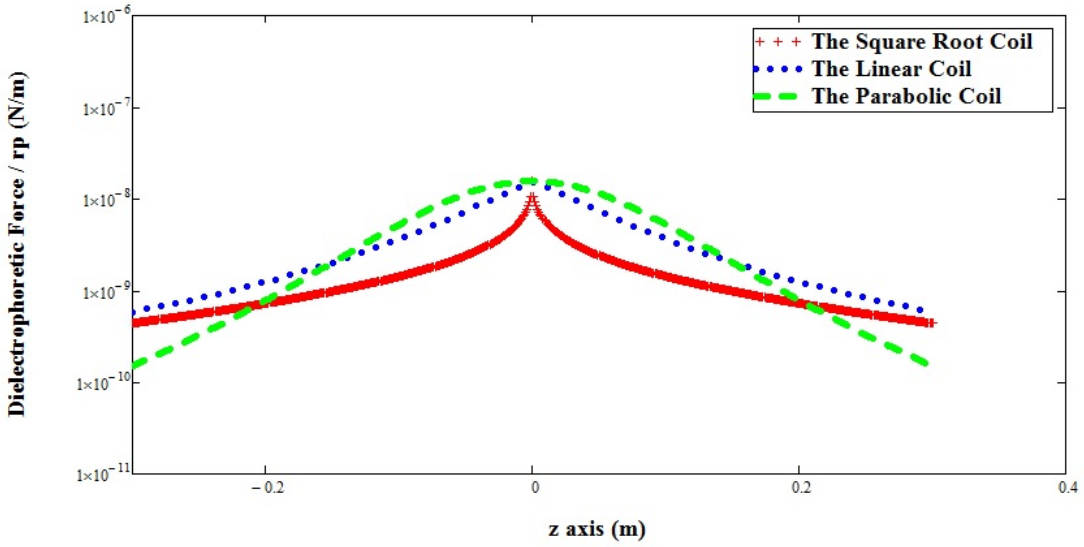

Figure 4.23 Comparison of the linear, the parabolic and the square root coil models (r1=15 cm and f=15 Hz)

Table 4.12
The Average Values of The DEPF/rp Inside The Linear, Parabolic and The Square Root Coils (r1=15 cm)

Coil Models	$\frac{DEPF\,(5Hz)}{rp}\ \frac{N}{m}$	$\frac{DEPF\,(10Hz)}{rp}\ \frac{N}{m}$	$\frac{DEPF\,(15Hz)}{rp}\ \frac{N}{m}$
$z = 0.1x^2 + 15\,(cm)$	5.50×10^{-8}	4.03×10^{-8}	1.41×10^{-8}
$z = x + 15\,(cm)$	9.73×10^{-8}	7.43×10^{-8}	2.55×10^{-8}
$z = \sqrt{x} + 15\,(cm)$	1.91×10^{-8}	1.39×10^{-8}	4.90×10^{-9}

Table 4.13
The Average Values of The DEPF Factor Inside The Linear, Parabolic and The Square Root Coils (r1=15 cm)

Coil Models	$\kappa_{DEPF}\,(5\,Hz)$	$\kappa_{DEPF}\,(10\,Hz)$	$\kappa_{DEPF}\,(15\,Hz)$
$z = 0.1x^2 + 15\,(cm)$	1.90	1.66	1.23
$z = x + 15\,(cm)$	1.70	1.53	1.18
$z = \sqrt{x} + 15\,(cm)$	1.31	1.23	1.08

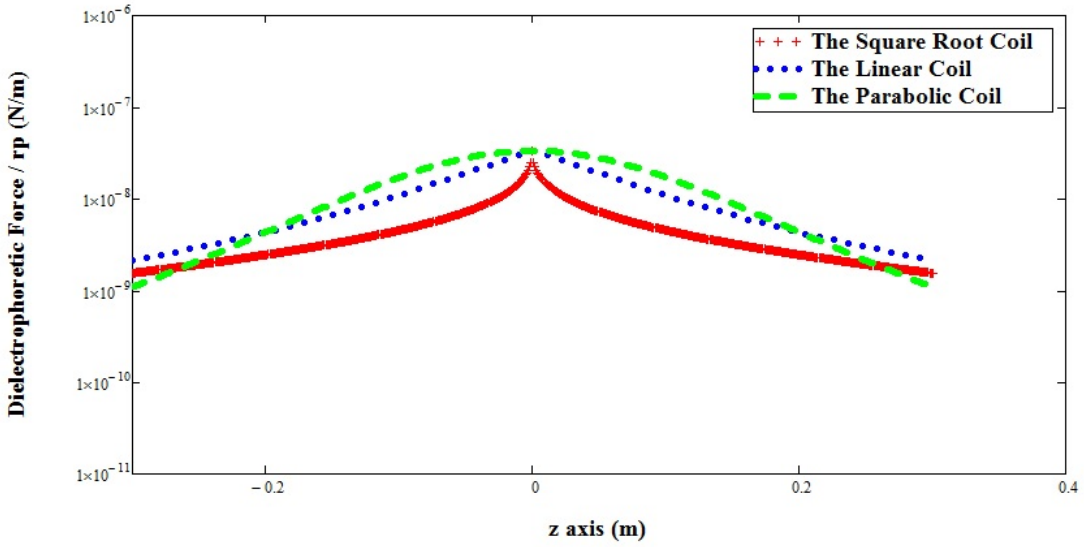

Figure 4.24 Comparison of the linear, the parabolic and the square root coil models (r1=20 cm and f=5 Hz)

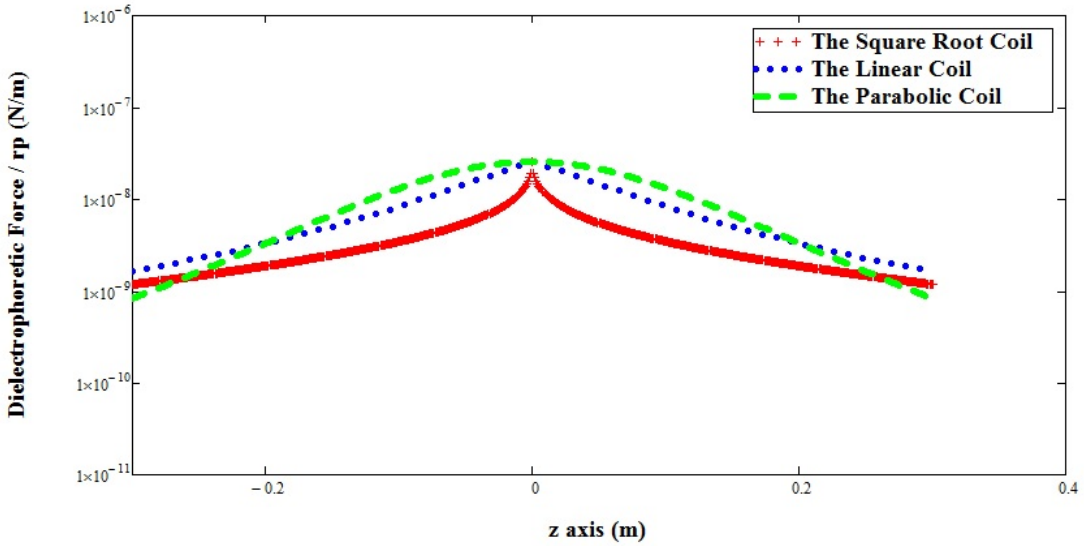

Figure 4.25 Comparison of the linear, the parabolic and the square root coil models (r1=20 cm and f=10 Hz)

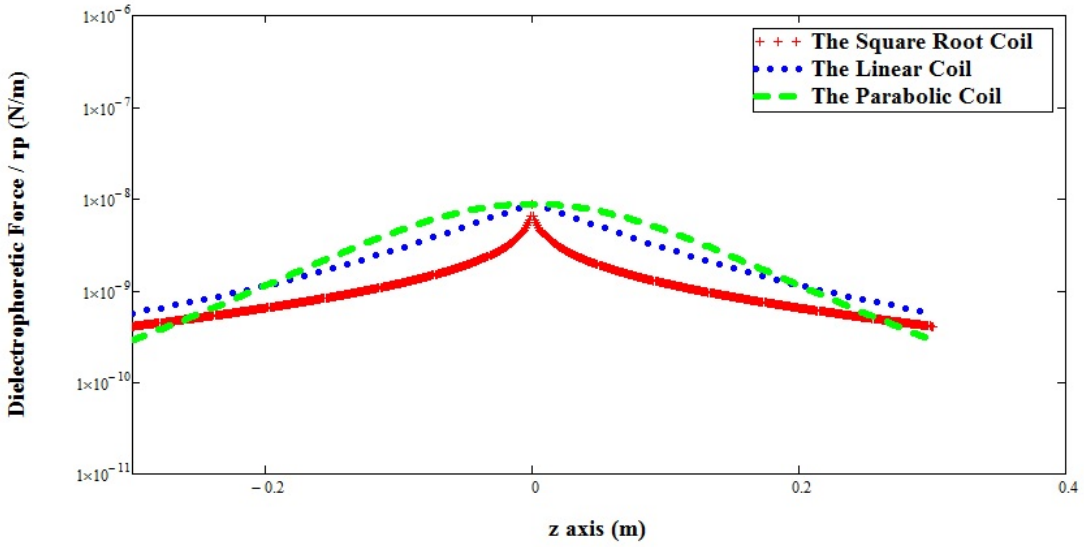

Figure 4.26 Comparison of the linear, the parabolic and the square root coil models (r1=20 cm and f=15 Hz)

Table 4.14
The Average Values of The DEPF/rp Inside The Linear, Parabolic and The Square Root Coils (r1=20 cm)

Coil Models	$\frac{DEPF\,(5Hz)}{rp}\ \frac{N}{m}$	$\frac{DEPF\,(10Hz)}{rp}\ \frac{N}{m}$	$\frac{DEPF\,(15Hz)}{rp}\ \frac{N}{m}$
$z = 0.1x^2 + 20\,(cm)$	3.75×10^{-8}	2.85×10^{-8}	9.93×10^{-9}
$z = x + 20\,(cm)$	1.16×10^{-8}	1.02×10^{-8}	7.35×10^{-9}
$z = \sqrt{x} + 20\,(cm)$	1.31×10^{-8}	1.04×10^{-8}	3.60×10^{-9}

Table 4.15
The Average Values of The DEPF Factor Inside The Linear, Parabolic and The Square Root Coils (r1=20 cm)

Coil Models	$\kappa_{DEPF}\,(5\,Hz)$	$\kappa_{DEPF}\,(10\,Hz)$	$\kappa_{DEPF}\,(15\,Hz)$
$z = 0.1x^2 + 20\,(cm)$	1.61	1.47	1.16
$z = x + 20\,(cm)$	1.26	1.17	1.12
$z = \sqrt{x} + 20\,(cm)$	1.21	1.17	1.06

Table 4.16
The Peak Values of The DEPF/rp Inside The Linear, The Parabolic and The Square Root Coils

At $z = 0$	$\frac{DEPF\,(5Hz)}{rp}\ \frac{N}{m}$	$\frac{DEPF\,(10Hz)}{rp}\ \frac{N}{m}$	$\frac{DEPF\,(15Hz)}{rp}\ \frac{N}{m}$
When $r1 = 10\,cm$	2.17×10^{-7}	1.66×10^{-7}	5.70×10^{-8}
When $r1 = 15\,cm$	9.73×10^{-8}	7.43×10^{-8}	2.55×10^{-8}
When $r1 = 20\,cm$	5.49×10^{-8}	4.19×10^{-8}	1.44×10^{-8}

Table 4.17
The Peak Values of The DEPF Factor for The Linear, Parabolic and The Square Root Coils

At $z = 0$	$\kappa_{DEPF}\,(5\,Hz)$	$\kappa_{DEPF}\,(10\,Hz)$	$\kappa_{DEPF}\,(15\,Hz)$
When $r1 = 10\,cm$	4.54	3.71	1.93
When $r1 = 15\,cm$	2.59	2.21	1.42
When $r1 = 20\,cm$	1.90	1.68	1.24

5. DISCUSSION AND CONCLUSIONS

Bone healing creates a demand for blood flow in tissues that are near the fracture site. Development of the vascular tissue and the initiation and propagation of the periosteal response are the prominent driving mechanism of bone regeneration. Vessel formation depends on sufficient blood flow. It has been well established that the increase of blood flow near the fracture site accelerates vessel formation and bone regeneration; a fracture may heal faster if there is an increase in the blood flow near the fracture site. A variety of techniques, including electrical stimulation, have been tried to facilitate fracture healing. For example, it has been shown that stimulation by direct current or ac current have beneficial effects. The exact mechanism by which electrical stimulation improves bone repair is still not fully understood. It needs more investigation. However, to date, direct current has been documented to work by an electrochemical reaction at the cathode, and capacitive coupling and inductive coupling have shown to work by alteration of growth factors and transmembrane signalling. Further studies are needed to support and optimize electrical stimulation for bone healing [3].

Since blood flow is extremely important for fracture healing, methods that can increase blood flow should also facilitate fracture healing. In the present thesis we studied how dielectrophoresis may help in this respect. The basic idea is to apply a non-uniform electromagnetic field around a fracture site and create electrical dipoles by the polarization of the red blood cells within the blood. Due to the interaction of these dipoles and the electromagnetic field, the red blood cells will be subjected to dielectrophoretic forces that will accelerate them and thus the blood flow will be increased. This will, in turn, increase vascularization, transmembrane signalling, the supply of nutrients, necessary hormones and growth factors at the fracture site and thus help bone fracture healing.

For the generation of non-uniform fields we considered three different coil designs (linear, parabolic and square root). Using Mathcad we numerically studied extensively, the dielectrophoretic forces for a long bone fracture where the main arteries are vertically-oriented and the blood flow is downward. The gravitational force and the drag force on the red blood cells determine the steady state blood flow. The dielectrophoretic force, added to the force balance is functional in increasing the blood flow.

Since the dielectrophoretic force is frequency dependent, it is important to determine the frequency range for which they are most effective. As seen in Figure 4.2, the DEPF reaches its peak level at a frequency between 5-15 Hz. In Section 4.3.4, the DEPF factor values for all the coil designs for 5 Hz, 10 Hz and 15 Hz are given. The peak values of the DEPF are the same for the square root, the linear and the parabolic coils. This is because the radii of the coils at the centers have same values. However, the average DEPF are different because the coils have different equations and different dimensions. Tables 4.10-4.15 give the average values of the DEPF/rp and the average values of the DEPF factor.

Figure 4.12 shows the DEPF vectors along the z and the r axes in cylindrical coordinates for the parabolic coil. It can be seen that the magnitute of the DEPF diminishes along the z axis. This demonstrates the gradient nature of the dielectrophoretic forces. Figure 4.13 shows a plot of the magnetic flux intensity along the z-axis at the center of the coils (r=0). When z=0, the magnitute peaks as desired.

The ratio of the velocity in the presence of dielectrophoresis to the velocity without dielectrophoresis (called here as the Dielectrophoretic Force Factor, κ_{DEPF}) is a good measure of the performance of the dielectrophoresis, since it indicates the increase in blood flow. It was found that the dielectorophoretic force reaches the peak levels at a frequency range between 5-15 Hz. At 5 Hz, the average value of κ_{DEPF} is 1.90, 2.51 and 1.61 for the linear, parabolic and the square root coils, respectively. Thus, the parabolic coil seems to be the best choice for bone healing.

5.1 Recommendations for Future Work

To use dielectrophoresis for bone healing, an adequate gradient electric field must created along the fracture site. This can be generated using various coil designs. In the present work, we have analyzed three coil designs (linear, parabolic and square root). We have found the parabolic coil to be the best choice for bone healing. However, different coil designs might lead to better results; this needs to be further investigated. Also, the effectiveness of the dielectrophoretic method must be tested experimentally on laboratory animals and on voluntered humans.

Appendix A. Derivation of Dielectrophoretic Force

In order to find the dielectrophoretic force, electric field inside the coil is calculated. Figure A.1 shows that the circular wire loop is considered in cylindrical coordinates. It is known the magnetic field inside the wire loop is:

$$\vec{B}_r(R, r_p, z_p) = \frac{\mu_0 I}{2\pi} \frac{z_p}{r_p \sqrt{(R + r_p)^2 + z_p^2}} \left[-K(k) + \frac{R^2 + r_p^2 + z_p^2}{(R - r_p)^2 + z_p^2} E(k) \right] \tag{A.1}$$

$$\vec{B}_z(R, r_p, z_p) = \frac{\mu_0 I}{2\pi} \frac{1}{r_p \sqrt{(R + r_p)^2 + z_p^2}} \left[K(k) + \frac{R^2 - r_p^2 - z_p^2}{(R - r_p)^2 + z_p^2} E(k) \right] \tag{A.2}$$

$$\vec{B}_\phi(R, r_p, z_p) = 0 \tag{A.3}$$

where K(k) and E(k) are elliptic integral of first and second kinds

$$K(k) = \int_0^1 \frac{1}{(1 - t^2)(1 - k^2 t^2)} dt \quad where \quad k^2 = \frac{4 R r_p}{(R + r_p)^2 + z_p^2} \tag{A.4}$$

$$E(k) = \int_0^1 \frac{\sqrt{1 - k^2 t^2}}{\sqrt{1 - t^2}} dt \quad where \quad k^2 = \frac{4 R r_p}{(R + r_p)^2 + z_p^2} \tag{A.5}$$

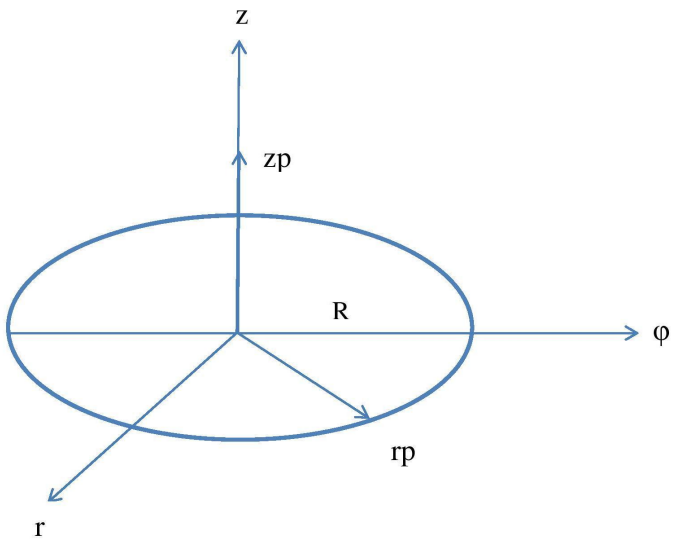

Figure A.1 Wire loop in the cylindrical coordinate system

$$\nabla \times \vec{B} = \left(\frac{1}{r}\frac{\partial B_z}{\partial \phi} - \frac{\partial B_\phi}{\partial z_p}\right)\vec{r} + \left(\frac{\partial B_r}{\partial z_p} - \frac{\partial B_z}{\partial r_p}\right)\vec{\phi} + \frac{1}{r}\left(\frac{\partial\left(rB_\phi\right)}{\partial r_p} - \frac{\partial B_r}{\partial \phi}\right)\vec{z} \qquad \text{(A.6)}$$

after calculations:

$$\nabla \times \vec{B} = \left(\frac{\partial B_r}{\partial z_p} - \frac{\partial B_z}{\partial r_p}\right)\vec{\phi} \qquad \text{(A.7)}$$

$$\frac{\partial B_z}{\partial r_p} = \frac{\mu_0 I}{2\pi}\left\{\left\{-\frac{(R+r_p)}{\left[(R+r_p)^2+z_p^2\right]^{\frac{3}{2}}}\right\}\left\{\int \frac{1}{(1-t^2)\left(1-\frac{4Rr_pt^2}{(R+r_p)^2+z_p^2}\right)}dt + \frac{R^2-r_p^2-z_p^2}{(R-r_p)^2+z_p^2}\int \frac{\sqrt{1-\frac{4Rr_pt^2}{(R+r_p)^2+z_p^2}}}{\sqrt{1-t^2}}dt\right\}\right.$$
$$+\left\{\int \frac{4Rt^2\left[(R+r_p)^2+z_p^2-2r_p(R+r_p)\right]}{(1-t^2)\left(1-\frac{4Rr_pt^2}{(R+r_p)^2+z_p^2}\right)^2\left[(R+r_p)^2+z_p^2\right]^2}dt\right.$$
$$-\frac{2r_p\left[(R+r_p)^2+z_p^2\right]+2(R-r_p)\left(R^2-r_p^2-z_p^2\right)}{\left[(R+r_p)^2+z_p^2\right]^2}\int \frac{\sqrt{1-\frac{4Rr_pt^2}{(R+r_p)^2+z_p^2}}}{\sqrt{1-t^2}}dt$$
$$\left.\left.-\frac{2Rt^2\left[(R+r_p)^2+z_p^2-2r_p(R+r_p)\right]}{\sqrt{1-t^2}\sqrt{1-\frac{4Rr_pt^2}{(R+r_p)^2+z_p^2}}\left[(R+r_p)^2+z_p^2\right]^2}\times\frac{R^2-r_p^2-z_p^2}{(R-r_p)^2+z_p^2}\right\}\right.$$
$$\left.\times\frac{1}{\sqrt{(R+r_p)^2+z_p^2}}\right\} \tag{A.8}$$

$$\frac{\partial B_r}{\partial z_p} = \frac{\mu_0 I}{2\pi}\left\{\frac{(R+r_p)^2}{r_p\left[(R+r_p)^2+z_p^2\right]^{\frac{3}{2}}}\left\{-\int \frac{1}{(1-t^2)\left(1-\frac{4Rr_pt^2}{(R+r_p)^2+z_p^2}\right)}dt + \frac{R^2+r_p^2+z_p^2}{(R-r_p)^2+z_p^2}\int \frac{\sqrt{1-\frac{4Rr_pt^2}{(R+r_p)^2+z_p^2}}}{\sqrt{1-t^2}}dt\right\}\right.$$
$$+\left\{\int \frac{8Rr_pz_pt^2}{(1-t^2)\left(1-\frac{4Rr_pt^2}{(R+r_p)^2+z_p^2}\right)^2\left[(R+r_p)^2+z_p^2\right]^2}dt\right.$$
$$+\frac{2z_p\left[(R-r_p)^2-R^2-r_p^2\right]}{\left[(R-r_p)^2+z_p^2\right]^2}\int \frac{\sqrt{1-\frac{4Rr_pt^2}{(R+r_p)^2+z_p^2}}}{\sqrt{1-t^2}}dt$$
$$+\int \frac{4Rr_pz_pt^2}{\sqrt{1-t^2}\sqrt{1-\frac{4Rr_pt^2}{(R+r_p)^2+z_p^2}}\left[(R+r_p)^2+z_p^2\right]^2}dt$$
$$\left.\left.\times\frac{R^2+r_p^2+z_p^2}{(R-r_p)^2+z_p^2}\right\}\frac{z_p}{r_p\sqrt{(R+r_p)^2+z_p^2}}\right\} \tag{A.9}$$

$$
\begin{aligned}
\nabla \times \vec{B} = \frac{\mu_0 I}{2\pi} \Bigg\{ & \frac{(R+r_p)^2}{r_p \left[(R+r_p)^2 + z_p^2\right]^{\frac{3}{2}}} \Bigg\{ - \int \frac{1}{(1-t^2)\left(1 - \frac{4Rr_p t^2}{(R+r_p)^2+z_p^2}\right)} dt \\
& + \frac{R^2 + r_p^2 + z_p^2}{(R-r_p)^2 + z_p^2} \int \frac{\sqrt{1 - \frac{4Rr_p t^2}{(R+r_p)^2+z_p^2}}}{\sqrt{1-t^2}} dt \Bigg\} \\
& + \Bigg\{ \int \frac{8Rr_p z_p t^2}{(1-t^2)\left(1 - \frac{4Rr_p t^2}{(R+r_p)^2+z_p^2}\right)^2 \left[(R+r_p)^2 + z_p^2\right]^2} dt \\
& + \frac{2z_p \left[(R-r_p)^2 - R^2 - r_p^2\right]}{\left[(R-r_p)^2 + z_p^2\right]^2} \int \frac{\sqrt{1 - \frac{4Rr_p t^2}{(R+r_p)^2+z_p^2}}}{\sqrt{1-t^2}} dt \\
& + \int \frac{4Rr_p z_p t^2}{\sqrt{1-t^2}\sqrt{1 - \frac{4Rr_p t^2}{(R+r_p)^2+z_p^2}} \left[(R+r_p)^2 + z_p^2\right]^2} dt \\
& \times \frac{R^2 + r_p^2 + z_p^2}{(R-r_p)^2 + z_p^2} \Bigg\} \frac{z_p}{r_p \sqrt{(R+r_p)^2 + z_p^2}} \Bigg\} \\
- \frac{\mu_0 I}{2\pi} \Bigg\{ & \Bigg\{ - \frac{(R+r_p)}{\left[(R+r_p)^2 + z_p^2\right]^{\frac{3}{2}}} \Bigg\} \Bigg\{ \int \frac{1}{(1-t^2)\left(1 - \frac{4Rr_p t^2}{(R+r_p)^2+z_p^2}\right)} dt \\
& + \frac{R^2 - r_p^2 - z_p^2}{(R-r_p)^2 + z_p^2} \int \frac{\sqrt{1 - \frac{4Rr_p t^2}{(R+r_p)^2+z_p^2}}}{\sqrt{1-t^2}} dt \Bigg\} \\
& + \Bigg\{ \int \frac{4Rt^2 \left[(R+r_p)^2 + z_p^2 - 2r_p (R+r_p)\right]}{(1-t^2)\left(1 - \frac{4Rr_p t^2}{(R+r_p)^2+z_p^2}\right)^2 \left[(R+r_p)^2 + z_p^2\right]^2} dt \\
& - \frac{2r_p \left[(R+r_p)^2 + z_p^2\right] + 2(R-r_p)\left(R^2 - r_p^2 - z_p^2\right)}{\left[(R+r_p)^2 + z_p^2\right]^2} \int \frac{\sqrt{1 - \frac{4Rr_p t^2}{(R+r_p)^2+z_p^2}}}{\sqrt{1-t^2}} dt \\
& - \frac{2Rt^2 \left[(R+r_p)^2 + z_p^2 - 2r_p (R+r_p)\right]}{\sqrt{1-t^2}\sqrt{1 - \frac{4Rr_p t^2}{(R+r_p)^2+z_p^2}} \left[(R+r_p)^2 + z_p^2\right]^2} \times \frac{R^2 - r_p^2 - z_p^2}{(R-r_p)^2 + z_p^2} \Bigg\} \\
& \times \frac{1}{\sqrt{(R+r_p)^2 + z_p^2}} \Bigg\} \phi
\end{aligned}
\tag{A.10}
$$

From maxwell equations, it is known that:

$$\vec{E} = \frac{\nabla \times \vec{B}}{\mu_0 \left(\sigma_\ell + \jmath\omega\epsilon_0\epsilon_r' + \omega\epsilon_0\epsilon_r''\right)} \tag{A.11}$$

Thus, putting $\left(\nabla \times \vec{B}\right)$ to the equation A.11 and taking the square of the final result, it is found square of the electric field. In order to calculate the dielectrophoretic force we must have the gradient of square of the electric field. After calculations, the gradient of square of the electric field is:

$$\begin{aligned}
\nabla E^2 = \frac{I^2}{2\pi} \{ & A \times B \times C^2 + C \times D \times A^2 + E \times F \times G^2 \\
& + G \times H \times E^2 + K \times L \times M^2 + M \times N \times K^2 + O \times P \times Q^2 - Q \times K \times O^2 \\
& + B \times C \times E \times G + A \times D \times E \times G + A \times C \times F \times G + A \times C \times E \times H \\
& + B \times C \times K \times M + A \times D \times K \times M + A \times C \times L \times M + A \times C \times K \times N \\
& - B \times C \times O \times Q - A \times D \times O \times Q - A \times C \times P \times Q + A \times C \times O \times K \\
& + F \times G \times K \times M + E \times H \times K \times M + E \times G \times L \times M + E \times G \times K \times N \\
& - F \times G \times O \times Q - E \times H \times O \times Q - E \times G \times P \times Q - E \times G \times O \times K \\
& - L \times M \times O \times Q - K \times N \times O \times Q - K \times M \times P \times Q + K \times M \times O \times K \\
& + A \times R \times C^2 + C \times S \times A^2 + E \times T \times G^2 + A \times G \times E^2 + K \times U \times M^2 \\
& + M \times V \times K^2 + O \times W \times Q^2 + Q \times X \times O^2 + R \times C \times E \times G \\
& + A \times S \times E \times G + A \times C \times T \times G + A \times C \times E \times A + R \times C \times K \times M \\
& + A \times S \times K \times M + A \times C \times U \times M + A \times C \times K \times V - R \times C \times O \times Q \\
& - A \times S \times O \times Q - A \times C \times W \times Q - A \times C \times O \times X + T \times G \times K \times M \\
& + E \times A \times K \times M + E \times G \times U \times M + E \times G \times K \times V - T \times G \times O \times Q \\
& - E \times A \times O \times Q + E \times G \times W \times Q - E \times G \times O \times X - U \times M \times O \times Q \\
& - K \times V \times O \times Q - K \times M \times W \times Q - K \times M \times O \times X \} \cdots
\end{aligned}$$

$$\cdots \div \left\{ \sigma_\ell^2 + 4\pi^2 f^2 \Im \left[-\epsilon_{r\infty} - \sum_{i=1}^{4} \frac{\epsilon_{ri}}{1 + (\jmath 2\pi f \tau_i)^{\alpha_i}} \right]^2 \right.$$
$$-4\pi^2 f^2 \Re \left[\epsilon_{r\infty} + \sum_{i=1}^{4} \frac{\epsilon_{ri}}{1 + (\jmath 2\pi f \tau_i)^{\alpha_i}} \right]^2$$
$$+4\sigma_\ell \pi f \Im \left[-\epsilon_{r\infty} - \sum_{i=1}^{4} \frac{\epsilon_{ri}}{1 + (\jmath 2\pi f \tau_i)^{\alpha_i}} \right]$$
$$+4\jmath\sigma_\ell \pi f \Re \left[\epsilon_{r\infty} + \sum_{i=1}^{4} \frac{\epsilon_{ri}}{1 + (\jmath 2\pi f \tau_i)^{\alpha_i}} \right]$$
$$+8\jmath\pi^2 f^2 \Re \left[\epsilon_{r\infty} + \sum_{i=1}^{4} \frac{\epsilon_{ri}}{1 + (\jmath 2\pi f \tau_i)^{\alpha_i}} \right]$$
$$\left. \times \Im \left[-\epsilon_{r\infty} - \sum_{i=1}^{4} \frac{\epsilon_{ri}}{1 + (\jmath 2\pi f \tau_i)^{\alpha_i}} \right] \right\}$$

where,

$$A = \frac{(R + r_p)^2}{r_p \left[(R + r_p)^2 + z_p^2 \right]^{\frac{3}{2}}} \tag{A.12}$$

$$B = \frac{2r_p (R + r_p) \left[(R + r_p)^2 + z_p^2 \right]^{\frac{3}{2}} - (R + r_p)^2 \left[(R + r_p)^2 + z_p^2 \right]^{\frac{3}{2}}}{r_p^2 \left[(R + r_p)^2 + z_p^2 \right]^3} - \frac{3r_p (R + r_p)^3 \sqrt{(R + r_p)^2 + z_p^2}}{r_p^2 \left[(R + r_p)^2 + z_p^2 \right]^3} \tag{A.13}$$

$$C = \int \frac{1}{(1 - t^2) \left(1 - \frac{4Rr_p t^2}{(R + r_p)^2 + z_p^2} \right)} dt + \frac{R^2 + r_p^2 + z_p^2}{(R - r_p)^2 + z_p^2} \int \frac{\sqrt{1 - \frac{4Rr_p t^2}{(R + r_p)^2 + z_p^2}}}{\sqrt{1 - t^2}} dt \tag{A.14}$$

$$
\begin{aligned}
D = & \int \frac{4Rt^2\left[(R+r_p)^2+z_p^2-2r_p\left(R+r_p\right)\right]}{(1-t^2)\left(1-\frac{4Rr_pt^2}{(R+r_p)^2+z_p^2}\right)^2\left[(R+r_p)^2+z_p^2\right]^2}dt \\
& + \frac{2r_p\left[(R-r_p)^2+z_p^2\right]+2(R-r_p)(R^2+r_p^2+z_p^2)}{\left[(R-r_p)^2+z_p^2\right]^2}\int \frac{\sqrt{1-\frac{4Rr_pt^2}{(R+r_p)^2+z_p^2}}}{\sqrt{1-t^2}}dt \\
& - \int \frac{2Rt^2\left[(R+r_p)^2+z_p^2-2r_p(R+r_p)\right]}{\sqrt{1-\frac{4Rr_pt^2}{(R+r_p)^2+z_p^2}}\sqrt{1-t^2}\left[(R+r_p)^2+z_p^2\right]^2}dt\frac{R^2+r_p^2+z_p^2}{(R-r_p)^2+z_p^2}
\end{aligned}
\tag{A.15}
$$

$$
\begin{aligned}
E = & \int \frac{8Rr_pz_pt^2}{(1-t^2)\left(1-\frac{4Rr_pt^2}{(R+r_p)^2+z_p^2}\right)^2\left[(R+r_p)^2+z_p^2\right]^2}dt \\
& + \frac{2z_p\left[(R-r_p)^2-R^2-r_p^2\right]}{\left[(R-r_p)^2-z_p^2\right]^2}\int \frac{\sqrt{1-\frac{4Rr_pt^2}{(R+r_p)^2+z_p^2}}}{\sqrt{1-t^2}}dt \\
& + \int \frac{4Rr_pz_pt^2}{\left[(R+r_p)^2+z_p^2\right]^2\sqrt{1-\frac{4Rr_pt^2}{(R+r_p)^2+z_p^2}}\sqrt{1-t^2}}dt\frac{R^2+r_p^2+z_p^2}{(R-r_p)^2+z_p^2}
\end{aligned}
\tag{A.16}
$$

$$
\begin{aligned}
F = & \int \frac{8Rz_p t^2\left(1-t^2\right)\left(1-\frac{4Rr_p t^2}{(R+r_p)^2+z_p^2}\right)^2\left[(R+r_p)^2+z_p^2\right]^2}{\left(1-t^2\right)^2\left(1-\frac{4Rr_p t^2}{(R+r_p)^2+z_p^2}\right)^4\left[(R+r_p)^2+z_p^2\right]^4}dt \\
& + \int \frac{16Rr_p z_p t^2\left(1-t^2\right)(A1)(A2)}{\left(1-t^2\right)^2\left(1-\frac{4Rr_p t^2}{(R+r_p)^2+z_p^2}\right)^4\left[(R+r_p)^2+z_p^2\right]^4}dt \\
& + \left\{ \frac{2z_p\left[-2\left(R-r_p\right)-2r_p\right]\left[(R-r_p)^2+z_p^2\right]^2}{\left[(R-r_p)^2+z_p^2\right]^4} \right. \\
& \left. + \frac{8z_p\left[(R-r_p)^2+z_p^2\right]\left(R-r_p\right)\left[(R-r_p)^2-R^2-r_p^2\right]}{\left[(R-r_p)^2+z_p^2\right]^4} \right\} \\
& \times \int \frac{\sqrt{1-\frac{4Rr_p t^2}{(R+r_p)^2+z_p^2}}}{\sqrt{1-t^2}}dt \\
& - \int \frac{2Rt^2\left[(R+r_p)^2+z_p^2-2r_p\left(R+r_p\right)\right]}{\sqrt{1-\frac{4Rr_p t^2}{(R+r_p)^2+z_p^2}}\sqrt{1-t^2}\left[(R+r_p)^2+z_p^2\right]^2}dt\frac{2z_p\left[(R-r_p)^2-R^2-r_p^2\right]}{\left[(R-r_p)^2+z_p^2\right]^2} \\
& + \int \frac{4Rz_p t^2\left[(R+r_p)^2+z_p^2\right]^2\sqrt{1-t^2}\sqrt{1-\frac{4Rr_p t^2}{(R+r_p)^2+z_p^2}}}{\left[(R+r_p)^2+z_p^2\right]^4\left(1-t^2\right)\left(1-\frac{4Rr_p t^2}{(R+r_p)^2+z_p^2}\right)}dt \\
& - \int \frac{16Rr_p z_p t^2\left(R+r_p\right)\left[(R+r_p)^2+z_p^2\right]\sqrt{1-t^2}\sqrt{1-\frac{4Rr_p t^2}{(R+r_p)^2+z_p^2}}}{\left[(R+r_p)^2+z_p^2\right]^4\left(1-t^2\right)\left(1-\frac{4Rr_p t^2}{(R+r_p)^2+z_p^2}\right)}dt \\
& + \int \frac{8R^2 r_p z_p t^4\left(1-t^2\right)\left[\left(R+r_p^2\right)^2+z_p^2-2r_p\left(R+r_p\right)\right]\left[(R+r_p)^2+z_p^2\right]^2}{\left[(R+r_p)^2+z_p^2\right]^4\left(1-t^2\right)\left(1-\frac{4Rr_p t^2}{(R+r_p)^2+z_p^2}\right)}dt \\
& \times \frac{R^2+r_p^2+z_p^2}{(R-r_p)^2+z_p^2} \\
& + \frac{2r_p\left[(R-r_p)^2+z_p^2\right]+2\left(R-r_p\right)\left(R^2+r_p^2+z_p^2\right)}{\left[(R-r_p)^2+z_p^2\right]^2} \\
& \times \int \frac{4Rr_p z_p t^2}{\left[(R-r_p)^2+z_p^2\right]^2\sqrt{1-t^2}\sqrt{1-\frac{4Rr_p t^2}{(R+r_p)^2+z_p^2}}}dt
\end{aligned}
\tag{A.17}
$$

$$
G = \frac{z_p}{r_p\sqrt{(R+r_p)^2+z_p^2}} \tag{A.18}
$$

$$H = -\frac{z_p\sqrt{\left(R+r_p\right)^2+z_p^2}+\frac{r_p(R+r_p)}{\sqrt{\left(R+r_p\right)^2+z_p^2}}}{r_p^2\left[\left(R+r_p\right)^2+z_p^2\right]} \tag{A.19}$$

$$K = \frac{R+r_p}{\left[\left(R+r_p\right)^2+z_p^2\right]^{\frac{3}{2}}} \tag{A.20}$$

$$L = \frac{\left[\left(R+r_p\right)^2+z_p^2\right]^{\frac{3}{2}}-3\left(R+r_p\right)\sqrt{\left(R+r_p\right)^2+z_p^2}}{\left[\left(R+r_p\right)^2+z_p^2\right]^3} \tag{A.21}$$

$$\begin{aligned} M = &\int \frac{1}{\left(1-t^2\right)\left(1-\frac{4Rr_pt^2}{\left(R+r_p\right)^2+z_p^2}\right)}dt \\ &+\frac{R^2-r_p^2-z_p^2}{\left(R-r_p\right)^2+z_p^2}\int\frac{\sqrt{1-\frac{4Rr_pt^2}{\left(R+r_p\right)^2+z_p^2}}}{\sqrt{1-t^2}}dt \end{aligned} \tag{A.22}$$

$$\begin{aligned} N = &\int \frac{4Rt^2\left[\left(R+r_p\right)^2+z_p^2-2r_p\left(R+r_p\right)\right]}{\left(1-t^2\right)\left(1-\frac{4Rr_pt^2}{\left(R+r_p\right)^2+z_p^2}\right)^2\left[\left(R+r_p\right)^2+z_p^2\right]^2}dt \\ -&\frac{2r_p\left[\left(R-r_p\right)^2+z_p^2\right]-2\left(R-r_p\right)\left(R^2-r_p^2-z_p^2\right)}{\left[\left(R-r_p\right)^2+z_p^2\right]^2}\int\frac{\sqrt{1-\frac{4Rr_pt^2}{\left(R+r_p\right)^2+z_p^2}}}{\sqrt{1-t^2}}dt \\ &+\int\frac{2Rt^2\left[\left(R+r_p\right)^2-z_p^2-2r_p\left(R+r_p\right)\right]}{\sqrt{1-t^2}\sqrt{1-\frac{4Rr_pt^2}{\left(R+r_p\right)^2+z_p^2}}\left[\left(R+r_p\right)^2+z_p^2\right]^2}dt\frac{R^2-r_p^2-z_p^2}{\left(R-r_p\right)^2+z_p^2} \end{aligned} \tag{A.23}$$

$$O = \int \frac{4Rt^2\left[\left(R+r_p\right)^2+z_p^2-2r_p\left(R+r_p\right)\right]}{\left(1-t^2\right)\left(1-\frac{4Rr_pt^2}{\left(R+r_p\right)^2+z_p^2}\right)^2\left[\left(R+r_p\right)^2+z_p^2\right]^2}dt$$
$$-\frac{2r_p\left[\left(R-r_p\right)^2+z_p^2\right]+2\left(R-r_p\right)\left(R^2-r_p^2-z_p^2\right)}{\left[\left(R-r_p\right)^2+z_p^2\right]^2}\int\frac{\sqrt{1-\frac{4Rr_pt^2}{\left(R+r_p\right)^2+z_p^2}}}{\sqrt{1-t^2}}dt \qquad \text{(A.24)}$$
$$-\frac{2Rt^2\left[\left(R+r_p\right)^2+z_p^2-2r_p\left(R+r_p\right)\right]\left(R^2-r_p^2-z_p^2\right)}{\sqrt{1-t^2}\sqrt{1-\frac{4Rr_pt^2}{\left(R+r_p\right)^2+z_p^2}}\left[\left(R+r_p\right)^2+z_p^2\right]^2\left[\left(R-r_p\right)^2+z_p^2\right]}$$

$$
\begin{aligned}
P = & \\
& \int \frac{4Rt^2\left[2\left(R+r_p\right)-2\left(R+2r_p\right)\left(1-t^2\right)\left[\left(R+r_p\right)^2+z_p^2\right]^2\left(1-\frac{4Rr_pt^2}{\left(R+r_p\right)^2+z_p^2}\right)^2\right]}{\left(1-t^2\right)^2\left(1-\frac{4Rr_pt^2}{\left(R+r_p\right)^2+z_p^2}\right)^4\left[\left(R+r_p\right)^2+z_p^2\right]^4}dt \\
& -\int \frac{4Rt^2\left[\left(R+r_p\right)^2+z_p^2-2r_p\left(R+r_p\right)\right]\left(1-t^2\right)\left(A3-A4\right)}{\left(1-t^2\right)^2\left(1-\frac{4Rr_pt^2}{\left(R+r_p\right)^2+z_p^2}\right)^4\left[\left(R+r_p\right)^2+z_p^2\right]^4}dt \\
& -\frac{2\left\{\left[\left(R-r_p\right)^2+z_p^2\right]-4r_p\left(R-r_p\right)\right\}\left[\left(R-r_p\right)^2+z_p^2\right]^2}{\left[\left(R-r_p\right)^2+z_p^2\right]^4}\int \frac{\sqrt{1-\frac{4Rr_pt^2}{\left(R+r_p\right)^2+z_p^2}}}{\sqrt{1-t^2}}dt \\
& +\frac{2\left\{2(R^2-r_p^2-z_p^2)+2r_p\left(R-rp\right)\right\}\left[\left(R-r_p\right)^2+z_p^2\right]^2}{\left[\left(R-r_p\right)^2+z_p^2\right]^4}\int \frac{\sqrt{1-\frac{4Rr_pt^2}{\left(R+r_p\right)^2+z_p^2}}}{\sqrt{1-t^2}}dt \\
& -\frac{8r_p\left(R-r_p\right)\left[\left(R-r_p\right)^2+z_p^2\right]^2}{\left[\left(R-r_p\right)^2+z_p^2\right]^4}\int \frac{\sqrt{1-\frac{4Rr_pt^2}{\left(R+r_p\right)^2+z_p^2}}}{\sqrt{1-t^2}}dt \\
& -\frac{8\left(R-r_p\right)^2\left[\left(R-r_p\right)^2+z_p^2\right]\left(R^2-r_p^2-z_p^2\right)}{\left[\left(R-r_p\right)^2+z_p^2\right]^4}\int \frac{\sqrt{1-\frac{4Rr_pt^2}{\left(R+r_p\right)^2+z_p^2}}}{\sqrt{1-t^2}}dt \\
& +\int \frac{2Rt^2\left[\left(R+r_p\right)^2+z_p^2-2r_p\left(R+r_p\right)\right]}{\sqrt{1-\frac{4Rr_pt^2}{\left(R+r_p\right)^2+z_p^2}}\sqrt{1-t^2}\left[\left(R+r_p\right)^2+z_p^2\right]^2}dt \\
& \times\frac{2r_p\left[\left(R-r_p\right)^2+z_p^2\right]+2\left(R-r_p\right)\left(R^2-r_p^2-z_p^2\right)}{\left[\left(R-r_p\right)^2+z_p^2\right]^2} \\
& -\frac{2Rt^2\left[\left(R+r_p\right)^2+z_p^2-2r_p\left(R+r_p\right)\right]}{\left(1-\frac{4Rr_pt^2}{\left(R+r_p\right)^2+z_p^2}\right)^{\frac{3}{2}}\left[\left(R+r_p\right)^2+z_p^2\right]^2} \\
& \times\frac{2Rt^2\left[\left(R+r_p\right)^2+z_p^2-2r_p\left(R+r_p\right)\right]\left(R^2-r_p^2-z_p^2\right)}{\left[\left(R+r_p\right)^2+z_p^2\right]^2\left[\left(R-r_p\right)^2+z_p^2\right]\sqrt{1-t^2}} \\
& -\frac{2Rt^2\left[2\left(R+r_p\right)-2(R+2r_p)\right]\left[\left(R+r_p\right)^2+z_p^2\right]^2}{\sqrt{1-\frac{4Rr_pt^2}{\left(R+r_p\right)^2+z_p^2}}\left[\left(R+r_p\right)^2+z_p^2\right]^4}\times A5 \\
& +\frac{8Rt^2\left(R+r_p\right)\left[\left(R+r_p\right)^2+z_p^2\right]\left[\left(R+r_p\right)^2+z_p^2-2r_p(R+r_p)\right]}{\sqrt{1-\frac{4Rr_pt^2}{\left(R+r_p\right)^2+z_p^2}}\left[\left(R+r_p\right)^2+z_p^2\right]^4}\times A5 \\
& +\frac{2Rt^2\left[\left(R+r_p\right)^2+z_p^2-2r_p\left(R+r_p\right)\right]}{\sqrt{1-\frac{4Rr_pt^2}{\left(R+r_p\right)^2+z_p^2}}\left[\left(R+r_p\right)^2+z_p^2\right]^2} \\
& \times\frac{2r_p\left[\left(R-r_p\right)^2+z_p^2\right]+2\left(R-r_p\right)\left(R^2-r_p^2-z_p^2\right)}{\left[\left(R+r_p\right)^2+z_p^2\right]^2\sqrt{1-t^2}}
\end{aligned}
\tag{A.25}
$$

$$Q = \frac{1}{\sqrt{\left(R + r_p\right)^2 + z_p^2}} \tag{A.26}$$

$$R = -\frac{3 z_p \left(R + r_p\right)^2 \sqrt{\left(R + r_p\right)^2 + z_p^2}}{r_p \left[\left(R + r_p\right)^2 + z_p^2\right]^3} \tag{A.27}$$

$$\begin{aligned} S = & \int \frac{8 R r_p z_p t^2}{\left(1 - t^2\right)\left(1 - \frac{4 R r_p t^2}{\left(R + r_p\right)^2 + z_p^2}\right)^2 \left[\left(R + r_p\right)^2 + z_p^2\right]^2} dt \\ & + \frac{2 z_p \left[\left(R - r_p\right)^2 - R^2 - r_p^2\right]}{\left[\left(R + r_p\right)^2 + z_p^2\right]^2} \int \frac{\sqrt{1 - \frac{4 R r_p t^2}{\left(R + r_p\right)^2 + z_p^2}}}{\sqrt{1 - t^2}} dt \\ & + \int \frac{4 R r_p z_p t^2}{\sqrt{1 - t^2}\sqrt{1 - \frac{4 R r_p t^2}{\left(R + r_p\right)^2 + z_p^2}}\left[\left(R + r_p\right)^2 + z_p^2\right]^2} dt \frac{R^2 + r_p^2 + z_p^2}{\left(R - r_p\right)^2 + z_p^2} \end{aligned} \tag{A.28}$$

$$
\begin{aligned}
T = & \int \frac{8Rr_pt^2}{(1-t^2)\left(1-\frac{4Rr_pt^2}{(R+r_p)^2+z_p^2}\right)^2\left[(R+r_p)^2+z_p^2\right]^2}dt \\
& -\int \frac{128R^2r_p^2z_p^2t^4+32Rr_pz_p^2t^2\left[(R+r_p)^2+z_p^2\right]\left(1-\frac{4Rr_pt^2}{(R+r_p)^2+z_p^2}\right)}{(1-t^2)\left(1-\frac{4Rr_pt^2}{(R+r_p)^2+z_p^2}\right)^3\left[(R+r_p)^2+z_p^2\right]^4}dt \\
& +\frac{\left(2-8z_p^2\right)\left[(R-r_p)^2-R^2-r_p^2\right]\left[(R-r_p)^2+z_p^2\right]^2}{\left[(R-r_p)^2+z_p^2\right]^2}\int \frac{\sqrt{1-\frac{4Rr_pt^2}{(R+r_p)^2+z_p^2}}}{\sqrt{1-t^2}}dt \\
& +\int \frac{4Rr_pz_pt^2}{\sqrt{1-t^2}\sqrt{1-\frac{4Rr_pt^2}{(R+r_p)^2+z_p^2}}\left[(R+r_p)^2+z_p^2\right]^2}dt\frac{2z_p\left[(R-r_p)^2-R^2-r_p^2\right]}{\left[(R-r_p)^2-z_p^2\right]^2} \\
& +\frac{4Rr_pt^2}{\sqrt{1-t^2}\sqrt{1-\frac{4Rr_pt^2}{(R+r_p)^2+z_p^2}}\left[(R+r_p)^2+z_p^2\right]^2}\times\frac{R^2+r_p^2+z_p^2}{(R-r_p)^2+z_p^2} \\
& -\frac{16Rr_pz_p^2t^2}{\sqrt{1-t^2}\sqrt{1-\frac{4Rr_pt^2}{(R+r_p)^2+z_p^2}}\left[(R+r_p)^2+z_p^2\right]^3}\times\frac{R^2+r_p^2+z_p^2}{(R-r_p)^2+z_p^2} \\
& -\frac{16R^2r_p^2z_p^2t^4}{\sqrt{1-t^2}\left(1-\frac{4Rr_pt^2}{(R+r_p)^2+z_p^2}\right)^{\frac{3}{2}}\left[(R+r_p)^2+z_p^2\right]^4}\times\frac{R^2+r_p^2+z_p^2}{(R-r_p)^2+z_p^2} \\
& +\frac{2z_p\left[(R-r_p)^2+R^2-r_p^2\right]}{\left[(R-r_p)^2+z_p^2\right]^2}\int \frac{4Rr_pz_pt^2}{\sqrt{1-t^2}\sqrt{1-\frac{4Rr_pt^2}{(R+r_p)^2+z_p^2}}\left[(R+r_p)^2+z_p^2\right]^2}dt
\end{aligned}
\tag{A.29}
$$

$$
U = -\frac{3z_p\left(R+r_p\right)\sqrt{\left(R+r_p\right)^2+z_p^2}}{\left[(R-r_p)^2-z_p^2\right]^3} \tag{A.30}
$$

$$
\begin{aligned}
V = & -\int \frac{8Rr_pz_pt^2}{\sqrt{1-t^2}\sqrt{1-\frac{4Rr_pt^2}{(R+r_p)^2+z_p^2}}\left[(R+r_p)^2+z_p^2\right]^2}dt \\
& -\frac{2z_p\left[(R-r_p)^2-r_p^2\right]}{\left[(R-r_p)^2+r_p^2\right]^2}\int \frac{\sqrt{1-\frac{4Rr_pt^2}{(R+r_p)^2+z_p^2}}}{\sqrt{1-t^2}}dt \\
& +\int \frac{4Rr_pz_pt^2}{\sqrt{1-t^2}\sqrt{1-\frac{4Rr_pt^2}{(R+r_p)^2+z_p^2}}\left[(R+r_p)^2+z_p^2\right]^2}dt\frac{R^2-r_p^2-z_p^2}{(R-r_p)^2+z_p^2}
\end{aligned}
\tag{A.31}
$$

$$
\begin{aligned}
W = & \int \frac{8Rz_p t^2}{(1-t^2)\left[1-\frac{4Rr_p t^2}{(R+r_p)^2+z_p^2}\right]^2\left[(R+r_p)^2+z_p^2\right]^2}dt \\
& -\int \frac{16Rz_p t^2\left[(R+r_p)^2+z_p^2-2r_p(R+r_p)\right]}{(1-t^2)\left[1-\frac{4Rr_p t^2}{(R+r_p)^2+z_p^2}\right]^2\left[(R+r_p)^2+z_p^2\right]^3}dt \\
& -\int \frac{256R^2 r_p z_p^2 t^4\left[(R+r_p)^2+z_p^2-2r_p(R+r_p)\right]}{(1-t^2)\left[1-\frac{4Rr_p t^2}{(R+r_p)^2+z_p^2}\right]^2\left[(R+r_p)^2+z_p^2\right]^3}dt \\
& -\frac{4z_p(2r_p-R)}{\left[(R-r_p)^2+z_p^2\right]^2}\int \frac{\sqrt{1-\frac{4Rr_p t^2}{(R+r_p)^2+z_p^2}}}{\sqrt{1-t^2}}dt \\
& +\frac{8r_p z_p}{\left[(R-r_p)^2+z_p^2\right]^2}\int \frac{\sqrt{1-\frac{4Rr_p t^2}{(R+r_p)^2+z_p^2}}}{\sqrt{1-t^2}}dt \\
& +\frac{8z_p(R-r_p)\left(R^2-r_p^2-z_p^2\right)}{\left[(R-r_p)^2+z_p^2\right]^3}\int \frac{\sqrt{1-\frac{4Rr_p t^2}{(R+r_p)^2+z_p^2}}}{\sqrt{1-t^2}}dt \\
& -\int \frac{4Rr_p z_p t^2}{\sqrt{1-t^2}\sqrt{1-\frac{4Rr_p t^2}{(R+r_p)^2+z_p^2}}\left[(R+r_p)^2+z_p^2\right]^2}dt \\
& \times\frac{2r_p\left[(R-r_p)^2+z_p^2\right]+2(R-r_p)\left(R^2-r_p^2-z_p^2\right)}{\left[(R-r_p)^2+z_p^2\right]^2} \\
& -\frac{2Rt^2\left[(R+r_p)^2+z_p^2-2r_p(R+r_p)\right]}{\left[1-\frac{4Rr_p t^2}{(R+r_p)^2+z_p^2}\right]^{\frac{3}{2}}\left[(R+r_p)^2+z_p^2\right]^2} \\
& \times\frac{2Rt^2\left[(R+r_p)^2+z_p^2-2r_p(R+r_p)\right]\left(R^2-r_p^2-z_p^2\right)}{\sqrt{1-t^2}\left[(R+r_p)^2+z_p^2\right]^2\left[(R-r_p)^2+z_p^2\right]} \\
& -\frac{4Rz_p t^2\left(R^2-r_p^2-z_p^2\right)}{\sqrt{1-t^2}\sqrt{1-\frac{4Rr_p t^2}{(R+r_p)^2+z_p^2}}\left[(R+r_p)^2+z_p^2\right]^2\left[(R-r_p)^2+z_p^2\right]} \\
& +\frac{8Rz_p t^2\left[(R+r_p)^2+z_p^2-2r_p(R+r_p)\right]\left(R^2-r_p^2-z_p^2\right)}{\sqrt{1-t^2}\sqrt{1-\frac{4Rr_p t^2}{(R+r_p)^2+z_p^2}}\left[(R+r_p)^2+z_p^2\right]^3\left[(R-r_p)^2+z_p^2\right]} \\
& +\frac{4Rz_p t^2\left[(R+r_p)^2+z_p^2-2r_p(R+r_p)\right]}{\sqrt{1-t^2}\sqrt{1-\frac{4Rr_p t^2}{(R+r_p)^2+z_p^2}}\left[(R+r_p)^2+z_p^2\right]^2\left[(R-r_p)^2+z_p^2\right]}
\end{aligned}
\tag{A.32}
$$

$$X = -\frac{z_p}{\left[\left(R + r_p\right)^2 + z_p^2\right]^{\frac{3}{2}}} \tag{A.33}$$

$$A1 = \left(1 - \frac{4Rr_p t^2}{\left(R + r_p\right)^2 + z_p^2}\right) \frac{4Rt^2\left[\left(R + r_p\right)^2 + z_p^2 - 2r_p\left(R + r_p\right)\right]}{\left[\left(R + r_p\right)^2 + z_p^2\right]^2} \tag{A.34}$$

$$A2 = \left[\left(R + r_p\right)^2 + z_p^2\right]^2 + 4\left[\left(R + r_p\right)^2 + z_p^2\right]\left(R + r_p\right)\left(1 - \frac{4Rr_p t^2}{\left(R + r_p\right)^2 + z_p^2}\right)^2 \tag{A.35}$$

$$A3 = 4\left(R + r_p\right)\left[\left(R + r_p\right)^2 + z_p^2\right]\left(1 - \frac{4Rr_p t^2}{\left(R + r_p\right)^2 + z_p^2}\right)^2 \tag{A.36}$$

$$A4 = 2\left(1 - \frac{4Rr_p t^2}{\left(R + r_p\right)^2 + z_p^2}\right) \frac{4Rt^2\left[\left(R + r_p\right)^2 + z_p^2 - 2r_p\left(R + r_p\right)\right]}{\left[\left(R + r_p\right)^2 + z_p^2\right]^2} \left[\left(R + r_p\right)^2 + z_p^2\right]^2 \tag{A.37}$$

$$A5 = \frac{R^2 - r_p^2 - z_p^2}{\left[\left(R - r_p\right)^2 + z_p^2\right]\sqrt{1 - t^2}} \tag{A.38}$$

Appendix B. Numerical Analysis

The dielectrophoretic force for coil models are given by;

$$
\begin{aligned}
F = 2\pi r_p^3 \epsilon_0 \epsilon_m \Re\left[K\left(\omega\right)\right] \frac{I^2}{2\pi} \{ & A \times B \times C^2 + C \times D \times A^2 + E \times F \times G^2 \\
& + G \times H \times E^2 + K \times L \times M^2 + M \times N \times K^2 + O \times P \times Q^2 - Q \times K \times O^2 \\
& + B \times C \times E \times G + A \times D \times E \times G + A \times C \times F \times G + A \times C \times E \times H \\
& + B \times C \times K \times M + A \times D \times K \times M + A \times C \times L \times M + A \times C \times K \times N \\
& - B \times C \times O \times Q - A \times D \times O \times Q - A \times C \times P \times Q + A \times C \times O \times K \\
& + F \times G \times K \times M + E \times H \times K \times M + E \times G \times L \times M + E \times G \times K \times N \\
& - F \times G \times O \times Q - E \times H \times O \times Q - E \times G \times P \times Q - E \times G \times O \times K \\
& - L \times M \times O \times Q - K \times N \times O \times Q - K \times M \times P \times Q + K \times M \times O \times K \\
& + A \times R \times C^2 + C \times S \times A^2 + E \times T \times G^2 + A \times G \times E^2 + K \times U \times M^2 \\
& + M \times V \times K^2 + O \times W \times Q^2 + Q \times X \times O^2 + R \times C \times E \times G \\
& + A \times S \times E \times G + A \times C \times T \times G + A \times C \times E \times A + R \times C \times K \times M \\
& + A \times S \times K \times M + A \times C \times U \times M + A \times C \times K \times V - R \times C \times O \times Q \\
& - A \times S \times O \times Q - A \times C \times W \times Q - A \times C \times O \times X + T \times G \times K \times M \\
& + E \times A \times K \times M + E \times G \times U \times M + E \times G \times K \times V - T \times G \times O \times Q \\
& - E \times A \times O \times Q + E \times G \times W \times Q - E \times G \times O \times X - U \times M \times O \times Q \\
& - K \times V \times O \times Q - K \times M \times W \times Q - K \times M \times O \times X \} \cdots
\end{aligned}
$$

$$\cdots \div \left\{ \sigma_\ell^2 + 4\pi^2 f^2 \Im \left[-\epsilon_{r\infty} - \sum_{i=1}^{4} \frac{\epsilon_{ri}}{1+(\jmath 2\pi f \tau_i)^{\alpha_i}} \right]^2 \right.$$
$$-4\pi^2 f^2 \Re \left[\epsilon_{r\infty} + \sum_{i=1}^{4} \frac{\epsilon_{ri}}{1+(\jmath 2\pi f \tau_i)^{\alpha_i}} \right]^2$$
$$+4\sigma_\ell \pi f \Im \left[-\epsilon_{r\infty} - \sum_{i=1}^{4} \frac{\epsilon_{ri}}{1+(\jmath 2\pi f \tau_i)^{\alpha_i}} \right]$$
$$+4\jmath\sigma_\ell \pi f \Re \left[\epsilon_{r\infty} + \sum_{i=1}^{4} \frac{\epsilon_{ri}}{1+(\jmath 2\pi f \tau_i)^{\alpha_i}} \right]$$
$$+8\jmath\pi^2 f^2 \Re \left[\epsilon_{r\infty} + \sum_{i=1}^{4} \frac{\epsilon_{ri}}{1+(\jmath 2\pi f \tau_i)^{\alpha_i}} \right]$$
$$\left. \times \Im \left[-\epsilon_{r\infty} - \sum_{i=1}^{4} \frac{\epsilon_{ri}}{1+(\jmath 2\pi f \tau_i)^{\alpha_i}} \right] \right\}$$

The multipliers of the DEPF are from appendix A and the DEPF equation is derived in order to simulate the DEPF/rp versus frequency graphs to observe its dispersive characteristics.

$$\vec{B}_r(r, z_p) = \frac{\mu_0 I}{2\pi} \frac{z_p}{r_p \sqrt{(zp^2 + x + r_p)^2 + z_p^2}}$$
$$- \int \frac{1}{(1-t^2)\left[1 - \frac{4(z_p^2+x)r_p}{(zp^2+x+r_p)^2+z_p^2} t^2\right]}$$
$$+ \frac{(zp^2+x)^2 + r_p^2 + z_p^2}{(zp^2+x-r_p)^2 + z_p^2} \int \frac{\sqrt{1 - \frac{4(zp^2+x)r_p t^2}{(zp^2+x+r_p)^2+z_p^2}}}{\sqrt{1-t^2}} dt \tag{B.1}$$

$$\vec{B}_z(r_p, z_p) = \frac{\mu_0 I}{2\pi} \frac{1}{r_p \sqrt{(zp^2 + x + r_p)^2 + z_p^2}} + \int \frac{1}{(1-t^2)\left[1 - \frac{4(z_p^2+x)r_p}{(zp^2+x+r_p)^2+z_p^2} t^2\right]} + \frac{(zp^2+x)^2 - r_p^2 - z_p^2}{(zp^2+x-r_p)^2 + z_p^2} \int \frac{\sqrt{1 - \frac{4(zp^2+x)r_p t^2}{(zp^2+x+r_p)^2+z_p^2}}}{\sqrt{1-t^2}} dt \tag{B.2}$$

Br and Bz in the equations B.1 and B.2 are derived for the magnetic flux intensity graphs.

$$\vec{B}_r(r, z_p) = \frac{\mu_0 I}{2\pi} \frac{z_p}{r_p \sqrt{(R + r_p)^2 + z_p^2}} - \int \frac{1}{(1-t^2)\left[1 - \frac{4Rr_p}{(R+r_p)^2+z_p^2} t^2\right]} + \frac{R^2 + r_p^2 + z_p^2}{(R-r_p)^2 + z_p^2} \int \frac{\sqrt{1 - \frac{4Rr_p t^2}{(R+r_p)^2+z_p^2}}}{\sqrt{1-t^2}} dt \tag{B.3}$$

$$\vec{B}_z(r_p, z_p) = \frac{\mu_0 I}{2\pi} \frac{1}{r_p \sqrt{(R + r_p)^2 + z_p^2}} + \int \frac{1}{(1-t^2)\left[1 - \frac{4Rr_p}{(R+r_p)^2+z_p^2} t^2\right]} + \frac{R^2 - r_p^2 - z_p^2}{(R-r_p)^2 + z_p^2} \int \frac{\sqrt{1 - \frac{4Rr_p t^2}{(R+r_p)^2+z_p^2}}}{\sqrt{1-t^2}} dt \tag{B.4}$$

$\overrightarrow{F_r}$ and $\overrightarrow{F_z}$ are used to show the direction of the DEPF/rp inside the linear, the parabolic and the square root coils. It is simulated the vector plot of the DEPF/rp for the r and the z axes.

$$\overrightarrow{F_r} = 2\pi r_p^3 \epsilon_0 \epsilon_m \Re\left[K\left(\omega\right)\right] \frac{I^2}{2\pi} \times \cdots$$

$$\cdots \left\{ + A \times R \times C^2 + C \times S \times A^2 + E \times T \times G^2 + A \times G \times E^2 + K \times U \times M^2 \right.$$
$$+ M \times V \times K^2 + O \times W \times Q^2 + Q \times X \times O^2 + R \times C \times E \times G$$
$$+ A \times S \times E \times G + A \times C \times T \times G + A \times C \times E \times A + R \times C \times K \times M$$
$$+ A \times S \times K \times M + A \times C \times U \times M + A \times C \times K \times V - R \times C \times O \times Q$$
$$- A \times S \times O \times Q - A \times C \times W \times Q - A \times C \times O \times X + T \times G \times K \times M$$
$$+ E \times A \times K \times M + E \times G \times U \times M + E \times G \times K \times V - T \times G \times O \times Q$$
$$- E \times A \times O \times Q + E \times G \times W \times Q - E \times G \times O \times X - U \times M \times O \times Q$$
$$\left. - K \times V \times O \times Q - K \times M \times W \times Q - K \times M \times O \times X \right\} \overrightarrow{r} \cdots$$

$$\cdots \div \left\{ \sigma_\ell^2 + 4\pi^2 f^2 \Im \left[-\epsilon_{r\infty} - \sum_{i=1}^{4} \frac{\epsilon_{ri}}{1 + \left(\jmath 2\pi f \tau_i\right)^{\alpha_i}} \right]^2 \right.$$
$$- 4\pi^2 f^2 \Re \left[\epsilon_{r\infty} + \sum_{i=1}^{4} \frac{\epsilon_{ri}}{1 + \left(\jmath 2\pi f \tau_i\right)^{\alpha_i}} \right]^2$$
$$+ 4\sigma_\ell \pi f \Im \left[-\epsilon_{r\infty} - \sum_{i=1}^{4} \frac{\epsilon_{ri}}{1 + \left(\jmath 2\pi f \tau_i\right)^{\alpha_i}} \right]$$
$$+ 4\jmath\sigma_\ell \pi f \Re \left[\epsilon_{r\infty} + \sum_{i=1}^{4} \frac{\epsilon_{ri}}{1 + \left(\jmath 2\pi f \tau_i\right)^{\alpha_i}} \right]$$
$$+ 8\jmath\pi^2 f^2 \Re \left[\epsilon_{r\infty} + \sum_{i=1}^{4} \frac{\epsilon_{ri}}{1 + \left(\jmath 2\pi f \tau_i\right)^{\alpha_i}} \right]$$
$$\left. \times \Im \left[-\epsilon_{r\infty} - \sum_{i=1}^{4} \frac{\epsilon_{ri}}{1 + \left(\jmath 2\pi f \tau_i\right)^{\alpha_i}} \right] \right\}$$

$$\overrightarrow{F_z} = 2\pi r_p^3 \epsilon_0 \epsilon_m \Re\left[K\left(\omega\right)\right] \frac{I^2}{2\pi} \left\{ A \times B \times C^2 + C \times D \times A^2 + E \times F \times G^2 \right.$$
$$+ G \times H \times E^2 + K \times L \times M^2 + M \times N \times K^2 + O \times P \times Q^2 - Q \times K \times O^2$$
$$+ B \times C \times E \times G + A \times D \times E \times G + A \times C \times F \times G + A \times C \times E \times H$$
$$+ B \times C \times K \times M + A \times D \times K \times M + A \times C \times L \times M + A \times C \times K \times N$$
$$- B \times C \times O \times Q - A \times D \times O \times Q - A \times C \times P \times Q + A \times C \times O \times K$$
$$+ F \times G \times K \times M + E \times H \times K \times M + E \times G \times L \times M + E \times G \times K \times N$$
$$- F \times G \times O \times Q - E \times H \times O \times Q - E \times G \times P \times Q - E \times G \times O \times K$$
$$\left. - L \times M \times O \times Q - K \times N \times O \times Q - K \times M \times P \times Q + K \times M \times O \times K \right\} \overrightarrow{z} \cdots$$

$$\cdots \div \left\{ \sigma_\ell^2 + 4\pi^2 f^2 \Im \left[-\epsilon_{r\infty} - \sum_{i=1}^{4} \frac{\epsilon_{ri}}{1 + \left(\jmath 2\pi f \tau_i\right)^{\alpha_i}} \right]^2 \right.$$
$$- 4\pi^2 f^2 \Re \left[\epsilon_{r\infty} + \sum_{i=1}^{4} \frac{\epsilon_{ri}}{1 + \left(\jmath 2\pi f \tau_i\right)^{\alpha_i}} \right]^2$$
$$+ 4\sigma_\ell \pi f \Im \left[-\epsilon_{r\infty} - \sum_{i=1}^{4} \frac{\epsilon_{ri}}{1 + \left(\jmath 2\pi f \tau_i\right)^{\alpha_i}} \right]$$
$$+ 4\jmath\sigma_\ell \pi f \Re \left[\epsilon_{r\infty} + \sum_{i=1}^{4} \frac{\epsilon_{ri}}{1 + \left(\jmath 2\pi f \tau_i\right)^{\alpha_i}} \right]$$
$$+ 8\jmath\pi^2 f^2 \Re \left[\epsilon_{r\infty} + \sum_{i=1}^{4} \frac{\epsilon_{ri}}{1 + \left(\jmath 2\pi f \tau_i\right)^{\alpha_i}} \right]$$
$$\left. \times \Im \left[-\epsilon_{r\infty} - \sum_{i=1}^{4} \frac{\epsilon_{ri}}{1 + \left(\jmath 2\pi f \tau_i\right)^{\alpha_i}} \right] \right\}$$

Bibliography

1. Khan K Brukner P. Bone healing on health24. *Clinical Sports Medicine*, pages 131–151, 1999.

2. Heaney RP Harris WH. Skeletal renewal and metabolic bone disease. *N Engl J Med*, 1969.

3. M. Griffin and A. Bayat. Electrical stimulation in bone healing: critical analysis by evaluating levels of evidence. *Eplasty*, 11, 2011.

4. Bruce Mills. *Poe, Fuller, and the mesmeric arts: transition states in the American Renaissance*. University of Missouri, 2006.

5. Eiichi Fukada and Iwao Yasuda. On the piezoelectric effect of bone. *J. Phys. Soc. Japan*, 12(10):1158–1162, 1957.

6. Marko S Markov. Pulsed electromagnetic field therapy history, state of the art and future. *The Environmentalist*, 27(4):465–475, 2007.

7. Marko S Markov. Expanding use of pulsed electromagnetic field therapies. *Electromagnetic Biology and Medicine*, 26(3):257–274, 2007.

8. Donald Mackenzie and Francis D Veninga. Reversal of delayed union of anterior cervical fusion treated with pulsed electromagnetic field stimulation: case report. *Southern medical journal*, 97(5):519–524, 2004.

9. Neil Kahanovitz. Electrical stimulation of spinal fusion: a scientific and clinical update. *The Spine Journal*, 2(2):145–150, 2002.

10. Jr Vert Mooney Simmons, James W and Ike Thackerl. Pseudarthrosis after lumbar spine fusion : non-operative salvage with pulsed electromagnetic fields. *American Journal of Orthopedics (Belle Mead, N.J)*, 27(30), 10 June 2010.

11. VERT MOONEY. A randomized double-blind prospective study of the efficacy of pulsed electromagnetic fields for interbody lumbar fusions. *Spine*, 15(7):708, 1990.

12. JD Currey. *Bones structure and mechanism.* Princeton university Press, New jersey 08540, 2002.

13. Z. Aziz A. Nather, HJC Ong. *Bone Grafts and Bone Substitutes: Basic Science and Clinical Applications.* World Scientific Publishing Company, 2005.

14. PA Hill. Bone remodelling. *Journal of Orthodontics*, 25(2):101–107, 1998.

15. I.F.T. Hernández-Gil, M.A.A. Gracia, M. Pingarrón, and L. Jerez. Physiological bases of bone regeneration ii. the remodeling process. *Med Oral Patol Oral Cir Bucal*, 11:E151–215, 2006.

16. HP Wiesmann U. Meyer. *Bone and Cartilage Engineering.* Springer, Verlag Berlin Heidelberg, 2006.

17. JL Hiatt LP Gartner. *Color Textbook of Histology.* Saunders, 2001.

18. H.I. Roach, J. Erenpreisa, and T. Aigner. Osteogenic differentiation of hypertrophic chondrocytes involves asymmetric cell divisions and apoptosis. *The Journal of cell biology*, pages 483–494, 1995.

19. C.T. Brighton and R.M. Hunt. Histochemical localization of calcium in the fracture callus with potassium pyroantimonate. possible role of chondrocyte mitochondrial calcium in callus calcification. *The Journal of bone and joint surgery. American volume*, 68(5):703, 1986.

20. A. Ron, I. Shur, R. Daniel, R.R. Singh, N. Fishelson, N. Croitoru, D. Benayahu, and Y. Shacham-Diamand. Dielectric screening of early differentiation patterns in mesenchymal stem cells induced by steroid hormones. *Bioelectrochemistry*, 78(2):161–172, 2010.

21. S.P. Bruder, D.J. Fink, and A.I. Caplan. Mesenchymal stem cells in bone development, bone repair, and skeletal regenaration therapy. *Journal of cellular biochemistry*, 56(3):283–294, 1994.

22. J.E. Aubin. Regulation of osteoblast formation and function. *Reviews in endocrine & metabolic disorders*, 2(1):81–94, 2001.

23. I. Shur, R. Solomon, and D. Benayahu. Dynamic interactions of chromatin-related mesenchymal modulator, a chromodomain helicase-dna-binding protein, with promoters in osteoprogenitors. *Stem Cells*, 24(5):1288–1293, 2006.

24. Makarand V Risbud, Michael Sittinger, et al. Tissue engineering: advances in in vitro cartilage generation. *TRENDS in Biotechnology*, 20(8):351–356, 2002.

25. D. Benayahu, Y. Kletter, D. Zipori, and S. Wientroub. Bone marrow-derived stromal cell line expressing osteoblastic phenotype in vitro and osteogenic capacity in vivo. *Journal of cellular physiology*, 140(1):1–7, 1989.

26. G.S. Stein and J.B. Lian. Molecular mechanisms mediating proliferation/differentiation interrelationships during progressive development of the osteoblast phenotype. *Endocrine reviews*, 14(4):424–442, 1993.

27. HJJ Verhaar, CA Damen, SA Duursma, and BAA Scheven. A comparison of the action of progestins and estrogen on the growth and differentiation of normal adult human osteoblast-like cells in vitro. *Bone*, 15(3):307–311, 1994.

28. JW Chow, JM Lean, and TJ Chambers. 17 beta-estradiol stimulates cancellous bone formation in female rats. *Endocrinology*, 130(5):3025–3032, 1992.

29. J. Chow, JH Tobias, KW Colston, and TJ Chambers. Estrogen maintains trabecular bone volume in rats not only by suppression of bone resorption but also by stimulation of bone formation. *Journal of Clinical Investigation*, 89(1):74, 1992.

30. T. Takano-Yamamoto and G.A. Rodan. Direct effects of 17 beta-estradiol on trabecular bone in ovariectomized rats. *Proceedings of the National Academy of Sciences*, 87(6):2172, 1990.

31. Q. Qu, M. Perälä-Heape, A. Kapanen, J. Dahllund, J. Salo, HK Väänänen, and P. Härkönen. Estrogen enhances differentiation of osteoblasts in mouse bone marrow culture. *Bone*, 22(3):201–209, 1998.

32. D.C. Anderson. Sex-hormone-binding globulin. *Clinical endocrinology*, 3(1):69–96, 1974.

33. J. Voldman. Dielectrophoretic traps for cell manipulation. *BioMEMS and biomedical nanotechnology*, pages 159–186, 2007.

34. EP Furlani. Continuous magnetophoretic separation of blood cells from plasma at the microscale. *Arxiv preprint arXiv:0705.1831*, 2007.

35. J. Voldman. Electrical forces for microscale cell manipulation. *Annu. Rev. Biomed. Eng.*, 8:425–454, 2006.

36. Rockwood and Green. *Rockwood and Green's Fractures in Adults.* Walters Kluwer, 2009.